Heritability of hippocampal functional and microstructural organisation

Şeyma Bayrak (1, 2, 3)*, Reinder Vos de Wael (4)*, H. Lina Schaare (1, 2), Benoit Caldairou (5), Andrea Bernasconi (5), Neda Bernasconi (5), Boris C. Bernhardt (4), Sofie L. Valk (1, 2)

(1) Otto Hahn Group Cognitive Neurogenetics, Max Planck Institute for Human Cognitive and Brain Sciences, Leipzig, Germany
(2) Institute of Neuroscience and Medicine (INM-7: Brain and Behavior), Research Centre Jülich, Jülich, Germany
(3) Department of Cognitive Neurology, University Hospital Leipzig and Faculty of Medicine, University of Leipzig, Leipzig, Germany.
(4) McConnell Brain Imaging Centre, Montreal Neurological Institute, McGill University, Montreal, Quebec, Canada
(5) Neuroimaging of Epilepsy Laboratory, McConnell Brain Imaging Centre, Montreal Neurological Institute, McGill University, Montreal, Quebec, Canada

Correspondence to Şeyma Bayrak
Email: bayrak@cbs.mpg.de

Keywords: hippocampus, hippocampal subfields, gradients, heritability, microstructure, functional connectivity

* *These authors contributed equally.*

Abstract

The hippocampal formation is an uniquely infolded anatomical structure in the medial temporal lobe and it is involved in a broad range of cognitive and emotional processes. It consists of anatomically and functionally different subfields, including the subiculum (SUB), cornu ammonis areas (CA), and the dentate gyrus (DG). However, despite ample research on learning and plasticity of the hippocampal formation, heritability of its structural and functional organization is not fully known. To answer this question, we extracted microstructurally sensitive neuroimaging (i.e., T1w/T2w ratios) and resting-state functional connectivity information along hippocampal subfield surfaces from a sample of healthy twins and unrelated individuals of the Human Connectome Project Dataset. Our findings robustly demonstrate that functional connectivity and local microstructure of hippocampal subfields are highly heritable. Second, we found marked covariation and genetic correlation between the microstructure of the hippocampal subfields and the isocortex, indicating shared genetic factors influencing the microstructure of the hippocampus and isocortex. In both structural and functional measures, we observed a dissociation of cortical projections across subfields. In sum, our study shows that the functional and structural organization of the hippocampal formation is heritable and has a genetic relation to divergent macroscale functional networks within the isocortex.

Introduction

The hippocampal formation is a heavily infolded region in the medial temporal lobe and involved in a broad range of cognitive processes such as memory [1–3], emotional reactivity [4], and stress resilience [5–7]. The hippocampal formation is considered part of the allocortex, a phylogenetically old region [8]. The allocortex presents a primitive cytoarchitecture with three cell layers, in contrast to the six-layered isocortex [9,10]. Importantly, the hippocampal formation consists of multiple subfields, or zones, starting at the subiculum (SUB) and moving outward to the hippocampus proper; the cornu ammonis (CA), and dentate gyrus (DG) [11–14]. These subfields have unique anatomical properties and participate differently in hippocampal circuitry. Consequently, their contributions to functional processes are likely distinct [15–17]. Also, anatomical hippocampal-cortical projections are extensive and they have different characteristics based on the position within the hippocampal formation [18,19]. Tracer studies in rodents have shown that the ventral hippocampus is anatomically connected to the olfactory regions, prefrontal cortex, and amygdala, while the dorsal hippocampus is connected to the retrosplenial cortex, mammillary bodies, and anterior thalamus [20,21]. This ventral-dorsal transition in rodents may relate to an anterior-posterior axis in humans [22,23]. Conversely, hippocampal infolding aligns with a medial-lateral axis followed by the subfields, suggesting another transitional axis driven by the intracortical microstructure [14,24]. Thus, the hippocampal formation could feature two major axes, one from anterior to posterior regions, and the other along its infolding from SUB via CA to DG.

In humans, hippocampal-cortical functional connectivity patterns at rest underscore functional organizational axes within the hippocampal formation, along which functional connectivity patterns vary. The anterior-posterior separation, so called *long axis* specialization, has also been observed in resting-state fMRI (rs-fMRI) functional connectomics [25–27]. A second axis referred to as the *transverse or medio-lateral axis* emphasises connectome differences in lateral and medial hippocampal portions [9,18,24,28]. The transverse axis may in part reflect transitions between subfields. In recent years, several groups have used dimension reduction techniques, commonly known as gradients, to provide a parsimonious account of hippocampal functional connectivity [29–31]. Gradient techniques allow a continuous description of the functional connectome compared to discrete network representations of the brain [32–34]. Using these

gradients, prior studies have found relationships of hippocampal functional connectivity with anatomical organization and microstructure [31], as well as performance on memory recollection [30], and pattern separation tasks [29]. It is possible such individual variations in function are due to genetic factors. Indeed, gene expression has been observed to vary as a function of the anterior-posterior axis along the hippocampus [35]. Moreover, hippocampal subfield volumes have been shown to be significantly heritable [36] and to have genetic overlap with the total brain volume [37]. Subfield volumes have been associated with specific genomic loci and correlate genetically with schizophrenia, specifically the subiculum [38]. Taken together: 1) subtle variations in structural and functional organization of hippocampal subfields may be described by gradients; 2) average gene expression varies along an anterior posterior gradient; 3) hippocampal volume is heritable, suggesting individual variations in volume are under genetic influences. However, the extent to which individual variation within subfield functional and structural organization is driven by genetic factors, is not completely understood.

Here, we studied the heritability of hippocampal functional organization and microstructure at the subfield level. Resting state (rs)-fMRI and high-resolution structural T1w images were selected from the twin design Human Connectome Project (HCP) S900 data release [39]. To probe functional organization, we first obtained the hippocampal-cortical functional connectivity (FC) for each subfield and then implemented an unsupervised dimension reduction technique on FC measures, yielding functional gradients [31,40]. Hippocampal microstructural features were addressed by projecting an *in vivo* proxy for myelination (T1w/T2w) on the subfield surfaces [41]. Heritability of hippocampal subfield function and structure was computed using the twin and sibling design of the HCP data [39]. Additionally, to assess the microstructural congruence between hippocampus and isocortex, we computed structural intensity covariance (SiC) of the T1w/T2w maps and the corresponding genetic correlation. Last, we explored whether functional and microstructural organization together underlie a common hippocampal axis. To do so, we obtained their multimodal gradient representations by fusing both modalities [42], and evaluated their association with large-scale cortical functional networks.

Results

Hippocampal-isocortical functional organization is heritable (Figure 1)

To study the heritability of hippocampal functional and microstructural organization we selected n = 709 healthy adults from the HCP S900 young adult release with complete structural and functional imaging data [39]. We first correlated the rs-fMRI time series of each subfield with the time series of isocortical parcels to compute the hippocampal-isocortical functional connectivity (FC) in our sample (**Fig. 1a**). We then mapped the FC on the isocortex, separately for the subiculum (SUB), CA1-3 (CA), and CA4-DG (DG) (**Fig. 1b**). The strongest functional coupling between hippocampal subfields and isocortex was found to be in the default-mode, somatomotor, visual, and limbic networks.

Next, we studied the impact of familial relatedness on hippocampal-isocortical functional couplings. Therefore, we ran heritability analyses [43] on hippocampal-isocortical FC maps (**Fig. 1c**). Heritability (h^2) of SUB-isocortex FC was the highest in ventromedial, posterior cingulate, and precuneus areas, linked to sensorimotor, limbic, and default mode functional networks respectively. A similar heritability pattern was observed for CA-isocortex FC, with highest heritability in sensorimotor and salience networks. For the DG-isocortex FC, compared to SUB- and CA-isocortex FC, we observed higher heritability in primary sensorimotor areas and the superior temporal lobe, associated with sensorimotor and dorsal attention functional networks. The h^2 values were found to be significant throughout most of the cortical areas using a likelihood ratio test (**Supplementary Fig. S3a)**.

To illustrate the spatial organization of subfield-specific FC, we derived hippocampal connectivity gradients, consistent with Vos de Wael (2018) (**Fig. 1d**). Each connectivity gradient represented a particular axis of FC. Gradient 1 (G1 (FC)) presented an anterior-posterior (A-P) axis across hippocampal subfields and explained 24% of the variance (**Supplementary Fig. S1b**), whereas Gradient 2 (G2 (FC)) described a medial-lateral (M-L) axis and explained 9% of the variance. Loadings of the M-L axis decreased from SUB to CA, and were minimal along the DG.

We also obtained the heritability of the A-P (h^2(G1)) and M-L (h^2(G2)) functional gradients (**Fig. 1e**). For SUB and CA, h^2(G1) was found to be modest (mean: 0.14, range: [0.06, 0.30] and mean: 0.13, range: [0, 0.26] respectively). However, it was low for DG (mean: 0.05, range [0, 0.16]). The second gradient, h^2(G2), was found to be low for all subfields (SUB: mean: 0.05, range: [0, 0.18], CA: mean: 0.08, range: [0, 0.31], and DG: mean: 0.00, range: [0, 0.04]). The heritability was significant (FDRq < 0.05) only for the anterior and posterior portions of the SUB-G1 (FC) and lateral portions of CA-G2 (FC) (**Supplementary Fig. S3c)**.

Finally, the gradient decomposition was implemented on the heritability scores of the subfield-isocortical FC (**Fig. 1f**). The primary gradient of the FC heritability G1 (h^2) did not reveal a consistent transition pattern along the subfields. However, the secondary gradient of the FC heritability G2 (h^2) depicted an anterior-posterior separation of the h^2profiles for SUB and DG. This indicates that there are differentiable heritable patterns of functional connectivity of anterior and posterior portions of hippocampal subfields to the isocortex.

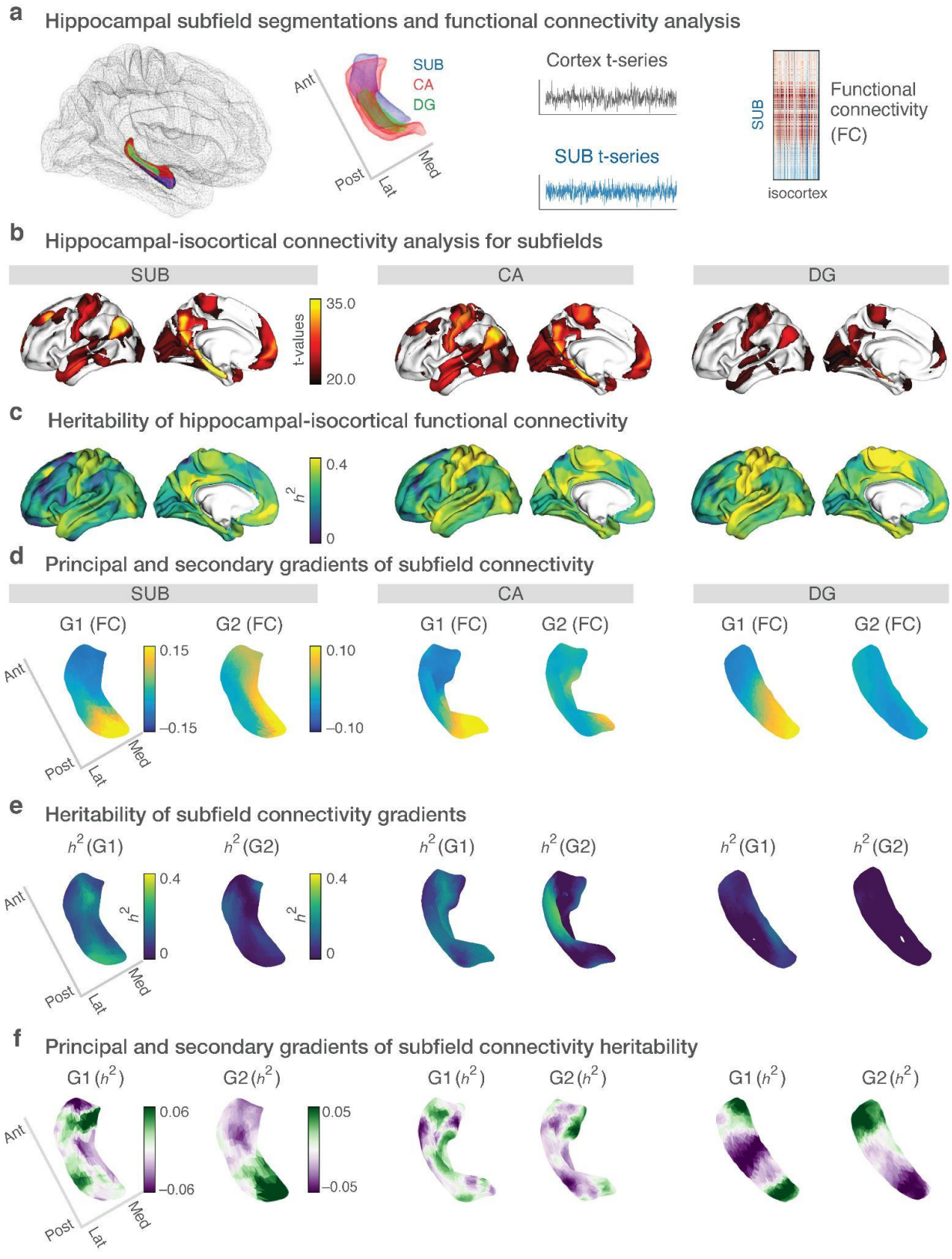

Fig. 1. Hippocampal-isocortical functional organization and its heritability. a. Subfield surfaces were automatically delineated using SurfPatch [44]: subiculum (SUB, blue), CA1-3 (CA, red), and CA4-DG (DG, green). Their rs-fMRI time series were extracted along the individual subfields and correlated with the time series of the isocortex to obtain subfield-isocortex functional connectivity (FC). **b.** Isocortex-wide FC of SUB (left), CA (middle), and DG (right). Isocortex-wide findings were thresholded at t > 20 to represent the highest connections. **c.** Heritability (h^2) of the hippocampal-isocortical FC throughout the isocortex. FC is the most heritable in ventromedial, posterior cingulate, and precuneus regions for SUB (left), with a similar pattern for CA (middle). For DG, heritability is the highest in sensorimotor cortex (right). **d.** Connectivity gradients of hippocampal-isocortical FC. Gradient 1 (G1 (FC)) depicts an anterior-posterior connectivity axis, whereas Gradient 2 (G2 (FC)) displays a medial-lateral axis. **e.** Heritability of subfield FC gradients (h^2(G1) and h^2(G2)). **f.** Gradients of hippocampal-isocortical FC heritability. Gradient 2 (G2 (h^2)) axis depicted an anterior-posterior separation of the h^2profiles for SUB and DG.

Heritability of hippocampal subfield microstructure (Figure 2)

To study the microstructural properties of the hippocampal subfields we used T1w/T2w intensity maps. Mean T1w/T2w intensity profiles distributed along the subfields did not reveal any potential outliers **(Fig. 2a)**. To evaluate the topographical relationship between functional organization and microstructural profiles, we correlated the secondary FC gradient (G2 (FC)) with the T1w/T2w maps for each subject (n = 709) and subfield in each individual **(Fig. 2b)**. Individual-level correlations were found to be significantly positive across participants for SUB ($\bar{r}$ = 0.53, p < 0.005, one-tailed Wilcoxon signed-rank test) and CA ($\bar{r}$ = 0.20, p < 0.005), however not for DG ($\bar{r}$ = -0.02, p = 0.21).

We also computed the heritability of these individual-level correlations and found them to be heritable in SUB and CA but not DG (SUB: h^2= 0.15, p = 0.030, CA: h^2= 0.15, p = 0.011, DG: h^2= 0.00, p = 0.5). We further quantified the group-level association between the T1w/T2w and G2 (FC) for subfields with Pearson correlations (r) and significance levels with the variogram approach (p_{vario}) [45] that controls for the spatial autocorrelations **(Fig. 2c)**. G2 (FC) had the strongest association with the T1w/T2w profiles for SUB (r = 0.93, p_{vario}< 0.001) and less with the other subfields (CA: r = 0.23, p_{vario}= 0.02, DG: r = -0.01, p_{vario}= 0.9). After correcting for the rs-fMRI temporal signal-to-noise ratio, the associations between T1w/T2w

profiles and G2 (FC) maps were preserved. This indicates a heritable correlation at individual and group levels between functional organisation and microstructure of SUB and CA.

Next, we aimed to evaluate whether the spatial variation of microstructure along the hippocampal subfields itself was heritable by computing heritability for the T1w/T2w intensity profile maps **(Fig. 2d)**. T1w/T2w maps were highly heritable across all subfields, reaching up to $h^2 = 0.77$ for SUB. Multiple comparison corrections using FDR reported significant heritability scores across almost all subfield vertices (100% of SUB vertices, 99% of CA and DG vertices). Similar heritability patterns for individual subfields, and both hemispheres, were found by adjusting for mean T1w/T2w as a covariate in the heritability model. This indicated that the heritability of subfields was present beyond any mean T1w/T2w intensity variation across individuals **(Supplementary Fig. S4)**.

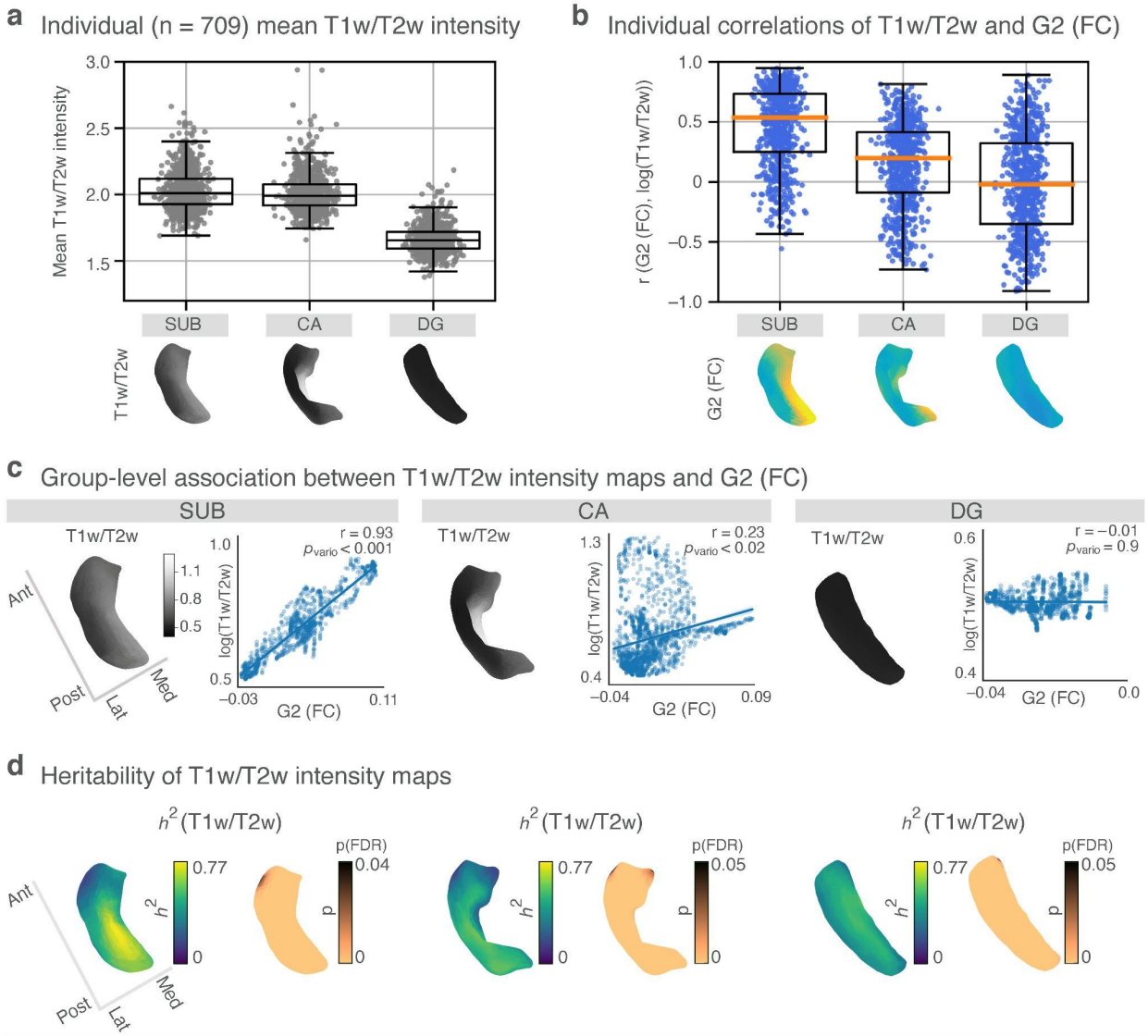

Fig. 2. Subfield T1w/T2w intensity maps, its association with the secondary FC gradient, and its heritability a. Mean T1w/T2w intensity profile distributions are demonstrated across participants (n = 709) and for each subfield (SUB, CA, DG). Mean and standard deviations of T1w/T2w maps were 2.02 ±0.41 for SUB, 2.01 ±0.78 for CA, and 1.66 ±0.22 for DG. **b.** Individual correlations (n = 709) between G2 (FC) maps and T1w/T2w intensity maps for each subfield. Individual correlations (r(G2 (FC) and log(T1w/T2w)) were significantly positive for the SUB (median $\bar{r}$ = 0.53, p < 0.005, one-tailed Wilcoxon signed-rank test) and CA ($\bar{r}$ = 0.20, p < 0.005), however not for DG ($\bar{r}$ = -0.02, p = 0.2). **c.** Group-level association between the mean T1w/T2w profiles and the G2 (FC) for each subfield. The T1w/T2w profiles of subfields correlate strongly with the G2 (FC) for SUB (r = 0.93 and p_{vario} < 0.001), however, not for the CA (r = 0.23 and p_{vario} = 0.02) or DG (r = -0.01 and p_{vario} = 0.9). **d.** Heritability of subfield T1w/T2w profiles (h^2(T1w/T2w)) and its significance levels p(FDR). T1w/T2w maps were strongly heritable across all subfields. p-values were reported after multiple comparison corrections using FDR (copper color denotes pFDR < 0.05, black pFDR > 0.05).

Hippocampal-isocortical structural intensity covariance and its genetic correlations (Figure 3)

Having shown that: 1) FC between hippocampal subfields and the isocortex is heritable and organised along the subfields and 2) microstructural organisation of hippocampal subfields is heritable, we explored whether the structural association between hippocampus and isocortex was associated with shared genetic factors. To uncover the microstructural similarity between hippocampal subfields and isocortex, we first computed the structural intensity covariance (SiC) of T1w/T2w maps across all participants (n = 709). We then evaluated its low-dimensional structure by means of dimension reduction [46] **(Fig. 3a)**. The principal gradient of SiC (G1 (SiC)) revealed an A-P organisational axis across all the subfields **(Fig. 3b)**. Further, we observed a high similarity between G1 (SiC) and G1 (FC) (SUB: Pearson's r = 0.89, CA: r = 0.88, and DG: r = 0.89). We found $p_{vario} < 0.001$ for all subfield G1 (SiC) and G1 (FC) similarities. The second gradient of SiC (G2 (SiC)) revealed a medial-lateral organisational axis, which was persistent across all subfields and corresponded to G2 (FC) in SUB and CA (SUB: r = 0.65, $p_{vario} < 0.001$, CA: r = 0.24, $p_{vario} = 0.02$, and DG: r = 0.16, $p_{vario} = 0.2$). Next, we assessed how hippocampal-isocortical SiC varies along the G1 (SiC) axis. First, the T1w/T2w of each isocortical parcel was correlated with T1w/T2w in each subfield vertex across participants. Then we evaluated the correspondence of the pattern of correlation between isocortex and for each subfield with G1 (SiC) **(Fig. 3c)**. By projecting the correlation coefficients (Pearson r-values) on the isocortex, we could study how hippocampal and isocortical regions spatially relate to each other in terms of their microstructural similarity. Anterior hippocampal portions (blue in **Fig. 3b**) shared more microstructural similarity with the anterior isocortex, while the posterior hippocampal portions (yellow in **Fig. 3b**) were more related to the posterior isocortex, particularly for SUB and CA. For the DG we observed less divergent patterns of subfield-isocortical similarity between its anterior and posterior portions.

Next, the genetic similarity of the hippocampal-isocortical SiC was obtained by computing the genetic correlation (GEN) of SiC and the decomposed axes of genetic correlation. The principal gradient of the genetic correlations between hippocampal and isocortical SiC (G1 (GEN)) displayed an A-P axis for SUB and CA, and an anteromedial-posterolateral axis for DG

(**Fig. 3d**). Similarities between G1 (GEN) and G1 (FC) were lower (SUB: r = 0.74, p_{vario}< 0.001, CA: r = 0.44, p_{vario}< 0.001, DG: r = 0.26, p_{vario}= 0.06) compared to similarities between G1 (SiC) and G1 (FC). The second gradient of GEN (G2 (GEN)) did not reveal a consistent organisational axis for SUB, however, an A-P axis for CA and DG was observed. Similar to SiC, we also investigated the correlation between hippocampal-isocortical GEN variations and G1 (GEN) (**Fig. 3e**). For SUB, anterior subfield portions (dark blue in **Fig. 3d**) shared more genetic similarity with the anterior isocortical apex, whereas posterior subfield portions (red in **Fig. 3d**) shared genetic similarity with primary sensory areas. For CA, anterior subfield portions were genetically more similar to the whole isocortex, except for the hippocampal-parahippocampal regions that shared genetic similarity with the posterior CA portions. For DG, anterior subfield portions shared more genetic similarity with the anterior isocortical apex including sensorimotor areas, while posterior portions were genetically correlated with parietotemporal areas. Thus, we showed differentiable patterns of genetic correlation between hippocampal and isocortical microstructure across the subfields. The posterior SUB was genetically similar to unimodal cortical domains, whereas posterior DG shared genetic similarity with posterior transmodal cortical domains.

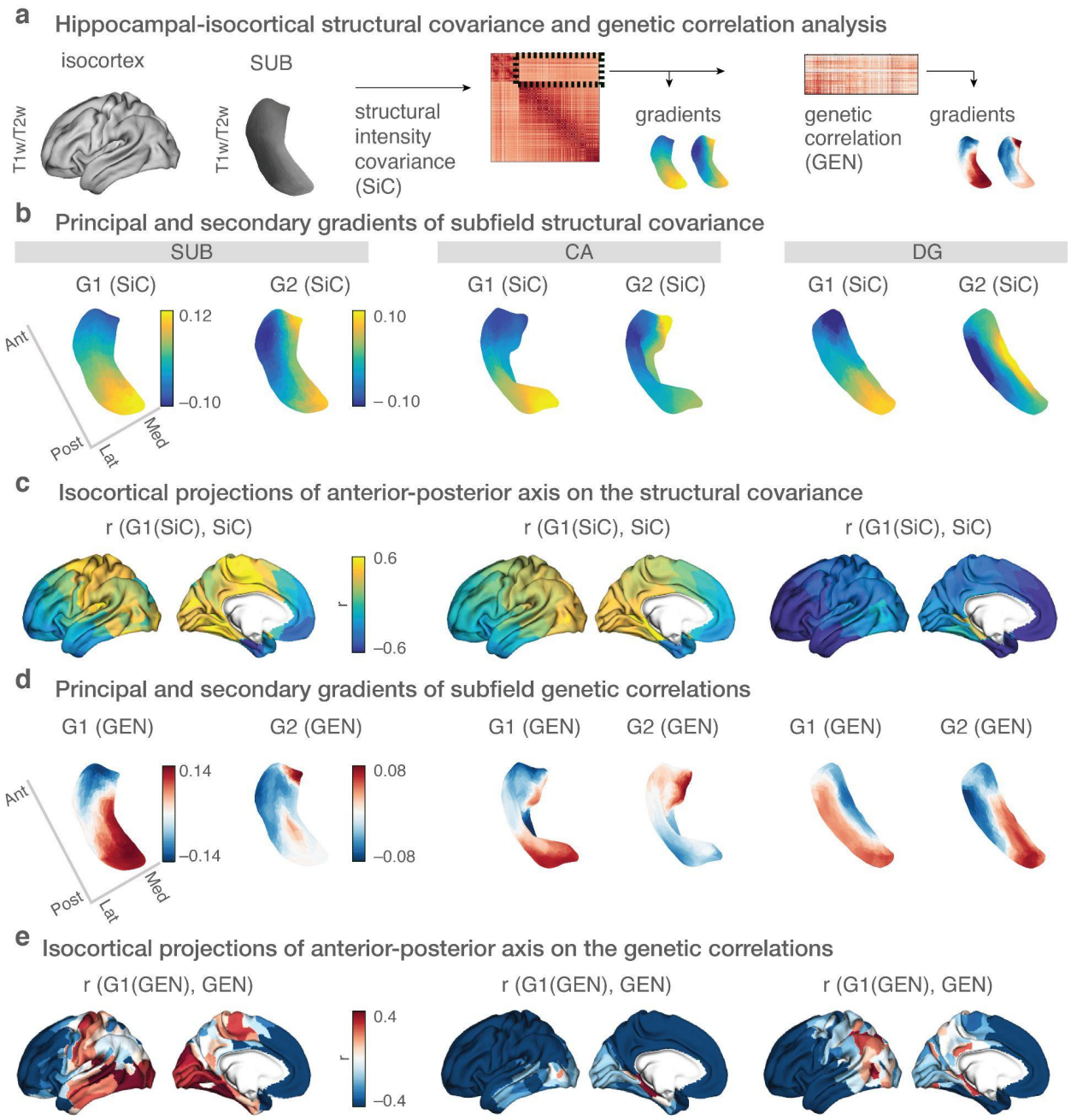

Fig. 3. Organization of hippocampal-isocortical structural intensity covariance (SiC) and its genetic correlations (GEN). a. The hippocampal-isocortical SiC was assessed by correlating hippocampal and isocortical T1w/T2w intensity maps across participants for each subfield. Here, the SiC matrix is depicted only for the SUB-isocortex associations for an exemplary demonstration. Shared genetic variations in T1w/T2w intensity maps were assessed by conducting a genetic correlation analysis. Both SiC and GEN matrices were then decomposed into their gradient representations, separately. **b.** Gradients of SiC for SUB (left), CA (middle), and DG (right). G1 (SiC) represents an anterior-posterior (A-P) axis of SiC, whereas G2 (SiC) depicts a medial-lateral (M-L) axis. **c.** Variations in SiC across its G1 (SiC) projected on the isocortex (Pearson's r-values). Lower r-values (blue) indicate SiC similarity between the

anterior subfield portions and isocortex, whereas higher r-values (yellow) that of the posterior subfield portions and isocortex. **d.** Gradients of GEN for SUB (left), CA (middle), and DG (right). G1 (GEN) represents an A-P axis for SUB and CA, whereas the DG axis is more posterolateral-anteromedially oriented. G2 (GEN) displays an A-P axis for CA and DG. **e.** Variations in GEN across its G1 (GEN) projected on the isocortex (Pearson's r-values). Lower r-values (dark blue) depict shared genetic influence between anterior subfield portions and isocortex and higher r-values (red) that of posterior subfield portions and isocortex.

Fused gradients of hippocampal-isocortical functional connectivity and structural intensity covariance (Figure 4)

To uncover a common organisational hippocampal axis shared by FC and SiC we next obtained the fused gradients by decomposing FC and SiC measures simultaneously (**Fig. 4a**). The principal fusion gradient $G1_{fus}$ emphasised anteromedial hippocampal portions for SUB and mediolateral portions for CA and DG, and show most resemblance to the patterns observed in G2 (FC) (SUB: r = 0.46, $p_{vario} < 0.001$, CA: r = 0.14, $p_{vario} = 0.11$, DG: r = 0.21, $p_{vario} = 0.03$) and G2 (SiC) (SUB: r = 0.39, $p_{vario} = 0.01$, CA: r = 0.74, $p_{vario} < 0.001$, DG: r = 0.36 and $p_{vario} = 0.004$). The second fused gradient $G2_{fus}$ revealed an A-P organisational axis for all subfields, which shared high similarity with G1 (FC) and G1 (SiC). Similarities between $G2_{fus}$ and G1 (FC) were reported as SUB: r = 0.89, CA: r = 0.89, DG: r = 0.86 and $p_{vario} < 0.001$ for all. Similarities between $G2_{fus}$ and G1 (SiC) were also reported for all subfields as SUB: r = 0.78, CA: r = 0.89, DG: r = 0.83 and $p_{vario} < 0.001$ for all (**Supplementary Table S1**).

We observed distinct variations in hippocampal-isocortical FC across the $G2_{fus}$ axis **(Fig. 4b)**, but not the $G1_{fus}$ axis **(Supplementary Fig. S5b)**. For the SUB, anterior subfield portions (blue in **Fig. 4a**) shared higher functional coupling with default mode network (DMN), sensorimotor, and limbic areas, whereas the posterior portions (yellow in **Fig. 4a**) showed higher functional coupling with fronto-parietal and salience domains (**Fig. 4c**). For CA and DG, the strength of functional coupling (r-values) decreased from the anterior subfield portions and increased and were more widely distributed for the posterior portions. Posterior subfield portions were most strongly connected to the dorsal attention and fronto-parietal areas for DG, whereas the coupling was lower towards CA and SUB.

Last, to assess the relationship between the hippocampal A-P axis and whole-brain intrinsic functional organisation, we obtained isocortical-isocortical FC gradients [34] (**Fig. 4d**). The principal isocortical gradient G1 (isocortex) reflects a sensory-transmodal axis, the second gradient G2 (isocortex) a visual-somatomotor axis, and the third gradient G3 (isocortex) the multiple demand axis versus sensorimotor and DMN networks. To quantify regional associations between hippocampal A-P axis and whole-brain gradients, we correlated the isocortical projections of the A-P axis (r($G2_{fus}$, FC)) and isocortical gradients (**Fig. 4e,** see **Supplementary Fig. S5b, S5c** for the r($G1_{fus}$, FC)). We observed that the A-P subfield axes showed consistent strong correlation with G3, dissociating multiple demand domains from sensorimotor and DMN functional networks (**Supplementary Table S2**). Correlation values were r = 0.82 (Pearson) for SUB, r = 0.79 for CA, and r = 0.73 for DG, and were found to be significant using spin permutation testing (p_{spin} [47]) for all subfields (p_{spin}< 0.001). At the same time, we observed inverse correlations of the A-P fused axes with isocortical G1 for CA (r = -0.30, p_{spin}= 0.002) and DG (r = -0.48, p_{spin}< 0.001), but not SUB (r = -0.06, p_{spin}= 0.6), driven by the differential relation of posterior and anterior subfield axes to visual and DMN networks. For the $G1_{fus}$ we again observed a negative relation to isocortical G1 for CA (r = -0.70, p_{spin}< 0.001) and DG (r = -0.54, p_{spin}< 0.001) but not SUB (r = 0.02, p_{spin}= 0.8). Here, medial/posterior regions related to sensory areas whereas more anterior/lateral subfield portions related to transmodal networks. Moreover, we observed that posterior/lateral regions showed a differential association with task-positive (SUB: r = -0.67, p_{spin}< 0.001) and task-negative (DG, r = 0.50, p_{spin}< 0.001) networks (based on isocortical G3) along this gradient ($G1_{fus}$), possibly reflecting variations with hippocampal infolding. These associations suggest that functional connectivity between hippocampal subfields and isocortex show meaningful variations between and within subfields and underscore the multifaceted association between hippocampal and isocortical organisation.

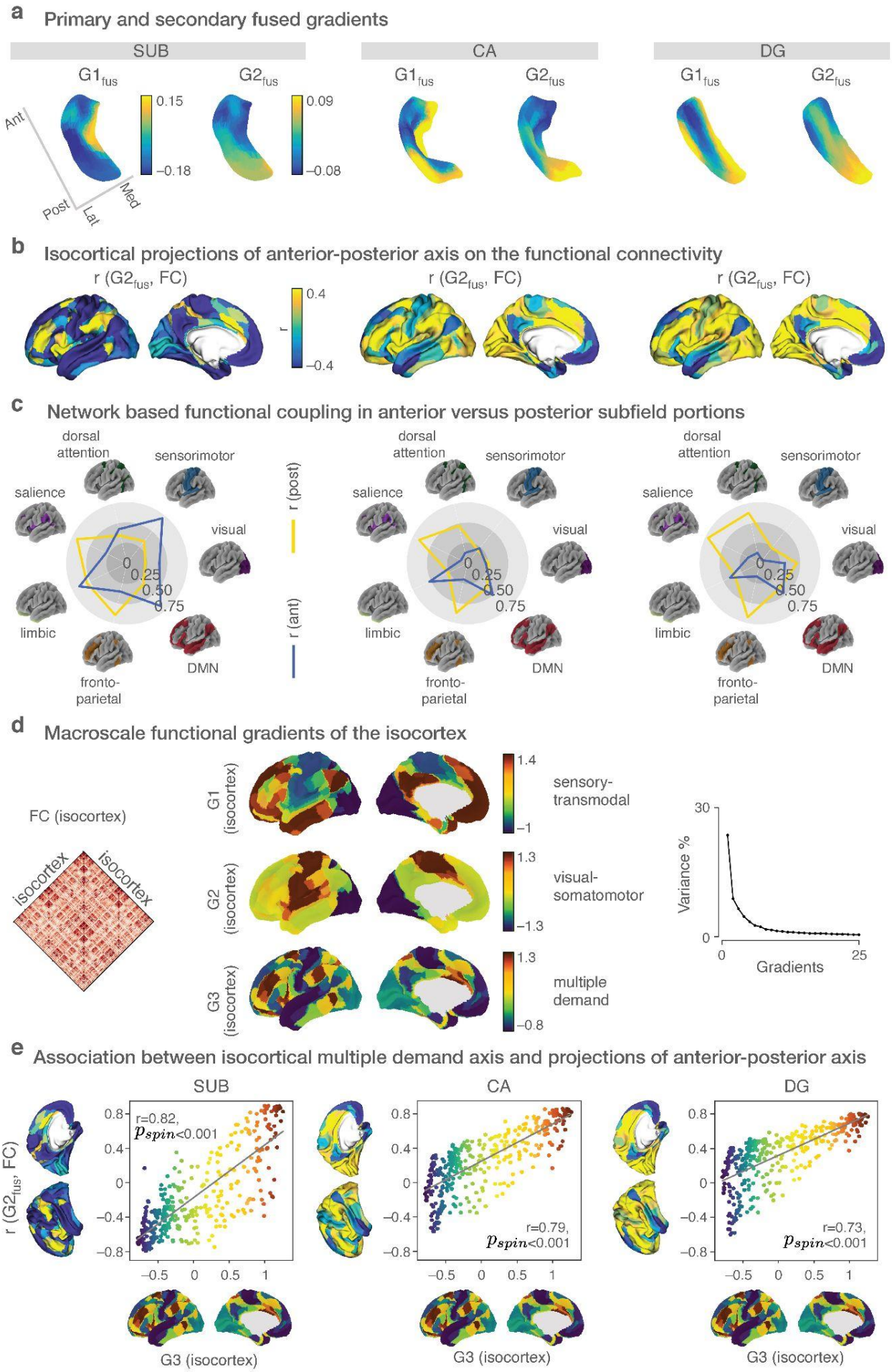

Fig. 4. Fused gradients of hippocampal-isocortical functional connectivity and structural intensity covariance. a. Gradient decomposition of hippocampal-isocortical *fused* functional connectivity (FC) and structural intensity covariance (SiC) revealed first and second fused gradients, $G1_{fus}$ and $G2_{fus}$, respectively for each subfield. The principal fusion gradient $G1_{fus}$ revealed the anterior-medial portions (yellow) for SUB (left), anterior-medial and posterior-lateral portions for CA (middle), and medial portions for DG (right). The second fused gradient $G2_{fus}$ displays an anterior-posterior axis for all subfields. **b.** Variations in hippocampal-isocortical FC across $G2_{fus}$ projected onto the isocortex (r-values). Lower r-values (blue) indicate functional coupling between anterior subfield portions and the isocortex, whereas higher r-values (yellow) depict that of posterior subfield portions and the isocortex. **c.** Findings in Panel B visualised across the seven networks [48]. **d.** Gradient decomposition of whole-brain isocortical-isocortical FC revealing G1 (isocortex), G2 (isocortex) and G3 (isocortex) and variance explained by the first 25 isocortical gradients. **e.** Regional associations between G3 (isocortex) (x-axis) and the r($G2_{fus}$, FC) from Panel B (y-axis), and their Pearson correlations (r) as well as the significance levels assessed by the spin permutation testing (p_{spin}, n_{perm} = 1000).

Discussion

The hippocampus is an anatomically unique structure that is considered to be a hub for cognitive and emotional processes. Here, we studied the heritability of functional organization and microstructure of the hippocampal formation and explored its genetic association with the isocortex. Building on emerging work describing the coalescence of multiple gradients of microstructure and function in the hippocampal formation *in vivo* [9,18,31,49], we provide several novel findings suggesting similar axes of heritability based on high definition neuroimaging data of the HCP S900. First, we found that functional coupling between hippocampal subfields and the isocortex was heritable. Second, subfield T1w/T2w intensity maps, serving as a marker for myelin-related microstructure, were also heritable and related to functional organisation. Moreover, we showed that structural intensity covariance of T1w/T2w between hippocampal subfields and isocortex followed an anterior-posterior (A-P) and a medial-lateral (M-L) axis. These patterns were genetically correlated, indicating that surface structure of the subfields underlie shared genetic influences with the isocortex. Decomposing fused functional connectivity (FC) and structural intensity covariance (SiC) measures, we again observed the A-P and M-L axes. Whereas the long-axis specialization was found to be linked to a functional axis describing on- versus off-task processing [50], the medial-lateral axis dissociated subfield patterns from sensory-to-attention versus sensory-to-DMN along hippocampal infolding. Taken together, we show that varying functional and microstructural properties within hippocampal subfields, and their relation to the isocortex, are under genetic influence. These patterns varied as a function of subfield, providing genetic evidence for differentiable system-level organization of hippocampal subfields.

To study the subregional organization of the hippocampal formation, we automatically segmented the hippocampal formation via a subfield and surface-based approach (SUB, CA, and DG) [44], which has been previously validated in both healthy individuals and those with hippocampal pathology [51]. Such surface-based approaches improve anatomical alignment across individuals [49]. Previously, animal studies have delineated the hippocampus into different zones based on its cytoarchitecture and attributed specific connectivity features to these zones [14]. Similar findings were reported in humans based on neurotransmitter distributions [11] and ex-vivo

MRI [9]. In the current work, we observed varying hippocampal-cortical functional connectivity (FC) profiles across subfields. The primary gradient G1 (FC) demonstrated A-P transitions (long axis [19,25–27]), whereas the secondary gradient G2 (FC) revealed M-L separations (transverse axis [18,24,28]). The A-P axis was equally predominant in all subfields. However, the M-L axis was the most distinct for the SUB. Further bridging the M-L axis and T1w/T2w maps, the M-L axis was found to align strongly with the microstructural proxy, particularly for the SUB and to a lesser extent in CA. In sum, the long axis specialization was preserved in all subfields, whereas the transverse axis indicated a link between intrinsic FC and microstructure, particularly in SUB.

Functional connectivity and structural organization of the hippocampal subfields was heritable, indicating individual variation was partly attributable to genetic factors. Hippocampal-isocortical FC was moderately heritable and its strength increased in the sensorimotor and dorsal attention domains from the SUB to CA and finally to DG. Studying the heritability within subfields we found that heritability estimates were highest within the subfield microstructure proxy (T1w/T2w) and lowest for the A-P (G1 (FC)) and M-L (G2 (FC)) functional hippocampal gradients. Indeed, the heritability of G1 (FC) and G2 (FC) itself was not significant, indicating that individual variation within functional gradients did not vary as a function of genetic proximity of individuals. At the same time we found that heritability of subfield-isocortical functional connectivity was again organised along an A-P axis, indicating that heritability of functional connectivity is different for anterior and posterior portions of hippocampal subfields. Quantifying the degree of heritability of the functional or structural properties of the brain could elevate our knowledge around the internal constraints shaping the brain. For instance, environmental influences on brain plasticity can be interpreted as a degree of aberration from the heritability of rs-fMRI connectivity, i.e. the less heritable the FC of a brain region, the larger the potential environmental influence [52–54]. It is thus possible that the low heritability of functional organization of subfields reflects these variations, attributable to environmental effects and associated hippocampal plasticity. Indeed, previous work in rodents and human adults has shown high plasticity of the hippocampus in both species [55], which has been linked to internal and external changes, such as hormonal levels and stress responses [56]. Conversely, the T1w/T2w microstructure along the hippocampal subfield surfaces were highly heritable. Previously, volume-based studies segmented the hippocampus into 12 subregions and

showed that these volumes exhibit strong heritability [36,57]. Here, we extended this work by studying the heritability of subtle variations of structure and function within subfield surfaces, as well as their link to the isocortex. Moreover, genome-wide studies identified single-nucleotide polymorphisms (SNP) associated with hippocampal volumes [58–60] showing, in part, unique SNPs for each subfield [61]. In line with these observations we also observed that each subfield had unique heritable patterns with the isocortex, as well as within the subfield itself. Such subtle within-subfield differences may help to understand the functional role of each subfield as well as its role in pathology, such as schizophrenia [38] and Alzheimer's disease [62], by further delineating meaningful variability in structure and function of hippocampal circuitry.

To understand whether T1w/T2w differentiation within hippocampal subfields was also related to variations in isocortex, we obtained structural intensity covariance (SiC) measures between the subfields and isocortex. SiC emphasises the morphological similarity among brain regions [63]. The primary and secondary gradients revealed A-P and M-L transitions, respectively. Although the decomposed SiC measure originated from the T1w/T2w maps, its low dimensional components depicted similar spatial organization to that of the functional maps. Furthermore, the subfield A-P axis overlapped congruently with the isocortical A-P axis. The anterior subfield portions were more similar to the anterior isocortical apex, whereas the posterior subfield portions were more similar to the posterior apex. This alignment with the isocortex was especially prominent for SUB and CA and diminished for DG. Earlier studies have presented an isocortex-wide A-P topography derived from cortical thickness morphology [64], microstructural profile covariance [65], and gray matter volumes [22]. Indeed, the isocortical A-P topography resembled the frontal-polar differentiation of myelin density [66,67]. Moreover, the A-P axis situates brain regions in coherence with their functional hierarchy, i.e. situated along a transmodal to unimodal axis, which also aligns with their neuronal density [67,68].

We also estimated genetic correlations (GEN) of SiC between hippocampal subfields and isocortex to evaluate the genetic association between hippocampal and cortical structure. Previous work has reported the topographical organization of the SiC to be genetically determined [69,70]. Thus, as for FC and SiC, the GEN measure was decomposed into its gradients as well. The primary genetic gradient (G1 (GEN)) revealed an A-P axis for SUB and CA and an anteromedial-posterolateral axis for the DG, whereas the secondary gradient (G2 (GEN)) did not

reveal a consistent pattern across subfields. Projecting the A-P genetic axis of subfields on the isocortex, we observed marked subfield differences. In general, the A-P genetic axis of SUB and DG was related to an A-P separation along the cortex as well. The concordance of genetic similarity between the A-P subfield axis and A-P isocortical axis were previously mirrored using transcriptomic data [35]. Here, we observed even more detailed transitions of genetic similarity between individual hippocampal subregions and cortex. For instance, the posterior SUB shared genetic similarity with the unimodal isocortical regions, whereas the posterior DG did so with the transmodal isocortical regions. Differences in subfield-isocortical genetic associations may indeed relate to the subfield specific neurodevelopmental trajectories, i.e. co-development of hippocampal subfields and isocortex. For example, the CA - Ammon's Horn - is one of the first brain regions to develop in the prenatal period [36,71] - revealed a more ambiguous genetic correlation pattern with the isocortex. Conversely, the SUB extends its maturation towards the postnatal period [72], dissociating anterior transmodal and unimodal regions. Finally, DG maturation exceeds the postnatal period [73], possibly underscoring posterior parietal associations. Thus, timing of pre- and post-natal development may be reflected in the genetic similarity patterning between subfields and isocortical functional domains.

Lastly, to better understand whether hippocampal function and structure underlie a common topographical pattern, we investigated multi-modal *fused* gradients $G1_{fus}$ and $G2_{fus}$. Whereas $G1_{fus}$ emphasised the medial or medial/lateral portions of subfields, $G2_{fus}$ depicted an A-P axis in all subfields similar to the primary gradients of FC and SiC. Indeed, $G1_{fus}$ may reflect a medial/lateral separation across the whole hippocampus, rather than the differentiation of individual subfields, which might emerge from the transverse axis formation as a result of cortical infolding. We observed that lateral SUB showed prominent association with multiple demand functional networks whereas the lateral DG showed association with DMN, a distinction possibly in line with previous work dissociating an iso-to-allocortical gradient along the mesial temporal lobe [9]. Second, anterior portions of the subfields presented on the $G2_{fus}$ axis were functionally connected to sensorimotor, DMN, and limbic cortices for the SUB. However, these connections became less prominent towards CA and DG. In contrast, posterior portions of the subfields were more strongly connected to fronto-parietal, dorsal-attention, and salience

domains, more prominently towards DG. These regional associations between the A-P axes across subfields were consistently associated with the third isocortical functional gradient, which represents the differentiation between on- and off-task processing [74]. On-task processing of the multiple demand system includes attention and control networks, responding to the environment, and is dissociated from off-task processing, typically linked to the DMN and internal thought [50,74]. Anterior subfield portions overlap with the DMN end of this gradient together with unimodal domains, whereas posterior subfield portions align with the fronto parietal end of G3 (isocortex). Such a pattern is in line with previous task-based functional studies. The anterior hippocampus has been reported to participate in associative memory processing [75], in which DMN is also involved and known to be integrating with parietal and temporal lobes for episodic memory retrieval [76]. Conversely the posterior hippocampus is suggested to be a mediator for spatial memory encoding [77], in which parietal cortices [78] and attention and salience networks are recruited [79]. Thus, the genetic divergence observed in function and structure between medial-to-lateral and anterior-to-posterior portions of hippocampal subfields may reflect differentiable functional systems, together dissociating associative and spatial memory.

In sum, we showed that functional and structural organisation hippocampal subfields is heritable and shows a genetic link to isocortical functional and structural organisation. Together these data expand previous notions on heritability of hippocampal structure and function at the individual level and underscore the functional relevance of such genetic axes. Future work may evaluate the association between maturational axes in cortical structure and divergent functional profiles along the hippocampal formation. This may provide an important step to better understand how the anatomy of the hippocampus supports its unique and versatile function.

Materials and Methods

Participants

Participants from the HCP S900 release [39] with four complete resting-state fMRI sessions and high-resolution structural images were selected (n = 822). Participants with anatomical anomalies or tissue segmentation errors listed in the HCP issues were discarded (n = 40). For every participant, we segmented hippocampal subfields: subiculum (SUB), CA1-3 (CA), and CA4-DG (DG) along the structural images using a patch-based surface algorithm [44]. Based on a visual inspection of subfield delineations, we discarded participants with poor segmentation quality (n = 42). As a necessity for the functional connectivity (FC) gradient analysis (see section **Functional Connectivity and Gradients**), we further excluded participants (n = 31), whose FC maps were poorly associated with the group-level reference FC. There remained n = 709 participants (395 women, mean ± SD age = 28.7 ± 3.7 y) accessible for our study. Among the 709 participants included in this study, there were 176 monozygotic twins, 178 siblings without twin status and 355 participants without familial relatedness. All quality assessment steps and analysis scripts used in this study are available at https://github.com/CNG-LAB/cngopen/tree/main/hippocampus.

Neuroimaging Data Acquisition and Preprocessing

Details of the HCP neuroimaging protocol and processing pipelines are available at Glasser (2013). In brief, we extracted T1-weighted (T1w) and T2-weighted (T2w) images available in the HCP initiative, which were all acquired on a 3T Siemens Skyra scanner. T1w images were acquired using a three-dimensional magnetization prepared rapid gradient-echo (3D-MPRAGE) sequence (0.7 mm isotropic voxels, matrix = 320×320, 256 sagittal slices, TR = 2400 ms, TE = 2.14 ms, TI = 1000 ms, flip angle = 8°, iPAT = 2). Resting-state fMRI images were acquired using a multi-band accelerated 2D-BOLD echo-planar imaging (EPI) sequence (2 mm isotropic voxels, matrix = 104×90, 72 sagittal slices, TR = 720 ms, TE = 33 ms, flip angle = 52°, mb factor = 8, 1200 volumes/scan). The fMRI data was collected at two sessions (1, 2) and

in two phase encoding directions at each session (left-right [LR] and right-left [RL]), resulting in four resting-state fMRI datasets in total ([LR1], [RL1], [LR2], [RL2]).

Preprocessing steps for the structural MRI images included gradient nonlinearity correction, brain extraction, distortion correction and coregistration of T1w and T2w images using rigid body transformations. Then, an intensity nonuniformity correction was performed using T1w and T2w contrasts [41] and subcortical structures were segmented using FSL FIRST [81]. Subsequently, preprocessed images were nonlinearly registered to the MNI152 template and cortical surfaces were reconstructed with FreeSurfer 5.3.0-HCP [82–84]. Finally, the individual cortical surfaces were registered to the Conte69 template [85] using MSMA11 [86].

Preprocessing of rs-fMRI images included corrections for the gradient nonlinearity, head motion and distortion. The images were then aligned to the T1w space using rigid-body and boundary-based registrations together [87]. The transformation matrices from this alignment step and that of the earlier T2w to T1w alignment were concatenated and applied to the rs-fMRI images at a single interpolation step to warp rs-fMRI images to the MNI152. Further processing in MNI152 space included bias field removal, whole brain intensity normalization, high pass filtering (>2000s FWHM) and noise removal with the ICA-FIX procedure [88].

Hippocampus Subfield Segmentations

We used the SurfPatch algorithm [44] to automatically delineate the hippocampal subfields of all participants: subiculum (SUB), CA1-3 (CA), and CA4-DG (DG). SurfPatch is a multi-template surface-path hippocampal segmentation method trained on a public dataset of manual segmentations in healthy controls [89], and has been validated in patients with histopathology of the hippocampus [51]. This algorithm incorporates a spherical harmonic shape parameterization and point distribution model of the surfaces [90]. Next, to minimise partial volume effects, we generated medial surfaces running through the center of each subfield using a Hamilton-Jakobian approach [91]. The spherical harmonic parameterization was propagated to the medial sheet to improve vertex-correspondence across individuals based on shape inherent information. Resultant CA surfaces consisted of 10242 vertices and both DG and SUB surfaces

of 5762 vertices. Next, CA, DG, and SUB surfaces were further downsampled to 2048, 1024, and 1024 vertices, respectively. All surface segmentations underwent a visual inspection and are available upon request.

Isocortex and Subfield Time Series

We mapped medial sheet meshes and volumetric resting-state fMRI data to native T1w space. Time series were sampled at each hippocampal and cortical mid-thickness vertex [86]. Hippocampal surface features were smoothed using a Gaussian diffusion kernel with 5 mesh units as FWHM in all subfields and isocortex. Sampling was carried out in a native T1w space to minimise the interpolation. Cortical time series were averaged within a previously established multi-modal parcellation scheme of the Glasser Atlas of 360 areas (180 regions per hemisphere) [86]. Surface-based time series were smoothed using a Gaussian diffusion kernel with 5 mesh units as full-width-at-half-maximum (FWHM).

Functional Connectivity

For every participant separately (n = 740), we computed the linear correlation coefficients between isocortex-wide time series (360×1200) and hippocampal subfield time series for SUB (1024×1200), CA (2048×1200), and DG (1024×1200). This resulted in a isocortex wide functional connectivity (FC) map (360×1) for every subject and subfield. We obtained group-level reference FC maps for every subfield by averaging individual FC maps across participants. We further profiled the similarity of individual FC maps to the reference FC maps by means of simple correlation (**Supplementary Fig. S1a**). Participants with a lower degree of similarity ($r < 0.45$) to the reference map were excluded (n = 31). Finally, the FC map of the isocortex to each hippocampal subfield for the remaining 709 participants was mapped using linear and mixed effects models in BrainStat (https://github.com/MICA-MNI/BrainStat).

T1w/T2w Maps and Structural Intensity Covariance

To study microstructural features of the hippocampus, we used the ratio of T1- over T2-weighted (T1w/T2w) image intensities. We resampled native T1w/T2w images to the MNI152 space and mapped them to hippocampal subfield surfaces (SUB, CA, DG) using Connectome Workbench (v1.4.2, volume-warpfield-resample and volume-to-surface-mapping tools) [92]. To assess the quality of T1w/T2w intensities projected on the hippocampal subfields, we obtained the mean T1w/T2w intensity distributions of all participants for potential outlier detection **(Fig. 2a, Supplementary Fig. S2c)**. We computed the structural intensity covariance (SiC) by correlating hippocampal and cortical T1w/T2w intensity maps resulting in 1384×1384 matrix for SUB, 2408×2408 matrix for CA, and 1384×1384 matrix for DG.

Heritability and Genetic Correlation

Heritability and genetic correlation analysis were conducted with the Sequential Oligogenic Linkage Analysis Routines (SOLAR, v8.5.1, http://www.solar-eclipse-genetics.org/). SOLAR employs a maximum likelihood variance-decomposition approach optimised to perform genetic analyses in pedigrees of arbitrary size and complexity [43,93]. SOLAR models genetic proximity by covariance between family members [43,93].

In brief, heritability (i.e. narrow-sense heritability h^2) is defined as the proportion of the phenotypic variance (σ_p^2) in a trait that is attributable to the additive effects of genes (σ_g^2), i.e. $h^2 = \sigma_g^2/\sigma_p^2$. SOLAR estimates heritability by comparing the observed phenotypic covariance matrix with the covariance matrix predicted by kinship [43,93]. Significance of the heritability estimate was tested using a likelihood ratio test where the likelihood of a restricted model (with σ_g^2 constrained to zero) is compared with the likelihood of the estimated model. Twice the difference between the log likelihoods of these models yields a test statistic, which is asymptotically distributed as a 50:50 mixture of a χ^2 variable with 1 degree-of-freedom and a point mass at zero [43,93]. We quantified the heritability of (i) hippocampal-isocortical functional connectivity patterns, (ii) hippocampal subfield gradients, and (iii) T1w/T2w intensity maps. We

included covariates in all heritability analyses including age, sex, $age \times sex$, age^2 and $age^2 \times sex$.

To estimate if variations in T1w/T2w intensity maps between hippocampus and isocortex were influenced by the same genetic factors, a genetic correlation analysis was conducted. Genetic correlations indicate the proportion of variance that determines the extent to which genetic influences on one trait are shared with genetic influences on another trait (e.g. pleiotropy). In SOLAR, the phenotypic correlation (ρ_p) was decomposed through bivariate polygenic analyses to estimate genetic (ρ_g) and environmental (ρ_e) correlations using the following formula: $\rho_p = \rho_g\sqrt{h_1^2 h_2^2} + \rho_e\sqrt{(1 - h_1^2)(1 - h_2^2)}$, where h_1^2 and h_2^2 are the heritability estimates of the vertex-based values in hippocampus and isocortex [94,95]. The significance of these correlations was determined (similar to heritability analyses) by likelihood ratio tests comparing a model in which ρ_g was estimated with a model in which ρ_g was constrained to zero (no shared genetic effect) and constrained to 1 (complete pleiotropy) [94,95].

Connectivity Gradients

We computed hippocampal subfield FC gradients, similarly to those identified by Vos de Wael (2018). Here, for every participant (n = 709), we first concatenated the subfield times series across SUB, CA, and DG. Next, the time series of each vertex was correlated with the isocortex wide time series, yielding a hippocampal-cortical FC map (4096×360) for every subject. We used BrainSpace [31,46] to derive connectivity gradients from the group-level FC matrix with the diffusion map embedding (normalised angle kernel, 90th percentile thresholding for the sparsity, and diffusion time estimation of $\alpha = 0.5$) [40]. This algorithm is in fact a manifold learning method that reveals underlying spatial variations in a connected graph, ie. in our case in the connectivity patterns of the hippocampal surfaces when moving from one vertex to another.

Using the diffusion embedding algorithm, we generated low-dimensional representations of hippocampal-cortical FC, namely the *gradients*. Along each single gradient (4096×1),

hippocampus vertices that share similar connectivity patterns have similar embedding values. The first and second gradients explained 32.4% of the total variance in the subfield FC map (**Supplementary Fig. S1b, S1c**). Having validated the gradient representations of hippocampal subfields at the group-level, we computed the individual-level gradients for every participant. Subsequently, individual gradients were aligned to the group-level gradients using Procrustes alignment to be scaled onto a common embedded connectivity space.

The gradients approach was further implemented on the heritability scores, structural intensity covariance (SiC), and genetic correlation measures individually, that aimed to characterise spatial motifs underlined by each of these modalities. We also implemented the *fused* gradients approach to identify whether different modalities support a common topographical motif together [42]. FC and SiC matrices were concatenated horizontally and rescaled to identical ranges to generate the *fused* data. This way we aimed to combine different modalities by still preserving the unique information in each. Secondly, performing the diffusion embedding manifold learning on the *fused* data, we obtained multimodal gradients driven by FC and SiC simultaneously.

Acknowledgements

We would like to thank the various contributors to the open access databases that our data was downloaded from. Funding: HCP data were provided by the Human Connectome Project, Washington University, the University of Minnesota, and Oxford University Consortium (Principal Investigators: David Van Essen and Kamil Ugurbil; 1U54MH091657) funded by the 16 NIH Institutes and Centers that support the NIH Blueprint for Neuroscience Research; and by the McDonnell Center for Systems Neuroscience at Washington University. This study was supported by the Deutsche Forschungsgemeinschaft (DFG, EI 816/21-1), the National Institute of Mental Health (R01-MH074457), the Helmholtz Portfolio Theme "Supercomputing and Modeling for the Human Brain" and the European Union's Horizon 2020 Research and Innovation Program under Grant Agreement No. 785907 (HBP SGA2). S.L.V was supported by Max Planck Gesellschaft (Otto Hahn award). B.C.B. acknowledges support from the SickKids Foundation (NI17-039), the National Sciences and Engineering Research Council of Canada (NSERC; Discovery-1304413), CIHR (FDN154298), Azrieli Center for Autism Research (ACAR), an MNI-Cambridge collaboration grant, and the Canada Research Chairs program. Last, this work was funded in part by Helmholtz Association's Initiative and Networking Fund under the Helmholtz International Lab grant agreement InterLabs-0015, and the Canada First Research Excellence Fund (CFREF Competition 2, 2015-2016) awarded to the Healthy Brains, Healthy Lives initiative at McGill University, through the Helmholtz International BigBrain Analytics and Learning Laboratory (HIBALL).

Author contributions

Ş.B., and S.L.V. conceived and designed the analysis, performed the analysis, wrote the draft manuscript and revised the manuscript. R.W. and H.L.S. aided in data analysis. A.B., B.C., N.B, R.W., and B.C.B. provided hippocampal subfield segmentations. All authors helped writing and revising the manuscript.

Competing interests

All co-authors declare no conflict of interests.

Materials & correspondence

This article is corresponding to Şeyma Bayrak (Ph.D. student, bayrak@cbs.mpg.de) and Dr. Sofie Valk (Ph.D., valk@cbs.mpg.de) at Cognitive Neurogenetics (CNG) lab, Max Planck Institute for Human Cognitive and Brain Sciences, Leipzig, Germany, and Research Center Jülich, Jülich, Germany.

References

1. Battaglia, F. P., Benchenane, K., Sirota, A., Pennartz, C. M. A. & Wiener, S. I. The hippocampus: hub of brain network communication for memory. *Trends Cogn. Sci.* **15**, 310–318 (2011).
2. Milner, B., Squire, L. R. & Kandel, E. R. Cognitive Neuroscience and the Study of Memory. *Neuron* vol. 20 445–468 (1998).
3. Squire, L. R. Memory and the hippocampus: a synthesis from findings with rats, monkeys, and humans. *Psychol. Rev.* **99**, 195–231 (1992).
4. Phelps, E. A. Human emotion and memory: interactions of the amygdala and hippocampal complex. *Curr. Opin. Neurobiol.* **14**, 198–202 (2004).
5. Franklin, T. B., Saab, B. J. & Mansuy, I. M. Neural mechanisms of stress resilience and vulnerability. *Neuron* **75**, 747–761 (2012).
6. Pruessner, J. C. *et al.* Stress regulation in the central nervous system: evidence from structural and functional neuroimaging studies in human populations - 2008 Curt Richter Award Winner. *Psychoneuroendocrinology* **35**, 179–191 (2010).
7. Lupien, S. J., McEwen, B. S., Gunnar, M. R. & Heim, C. Effects of stress throughout the lifespan on the brain, behaviour and cognition. *Nat. Rev. Neurosci.* **10**, 434–445 (2009).
8. Sanides, F. Die Architektonik des Menschlichen Stirnhirns. *Monographien aus dem Gesamtgebiete der Neurologie und Psychiatrie* (1962) doi:10.1007/978-3-642-86210-6.
9. Paquola, C. *et al.* Convergence of cortical types and functional motifs in the human mesiotemporal lobe. *Elife* **9**, (2020).
10. Insausti, R., Muñoz-López, M., Insausti, A. M. & Artacho-Pérula, E. The Human Periallocortex: Layer Pattern in Presubiculum, Parasubiculum and Entorhinal Cortex. A Review. *Front. Neuroanat.* **11**, 84 (2017).
11. Palomero-Gallagher, N., Kedo, O., Mohlberg, H., Zilles, K. & Amunts, K. Multimodal mapping and analysis of the cyto- and receptorarchitecture of the human hippocampus. *Brain Struct. Funct.* **225**, 881–907 (2020).
12. Wisse, L. E. M. *et al. A Harmonized Segmentation Protocol for Hippocampal and Parahippocampal Subregions: Why Do We Need One and what are the Key Goals?* (2017).
13. Yushkevich, P. A. *et al.* Quantitative comparison of 21 protocols for labeling hippocampal subfields and parahippocampal subregions in in vivo MRI: towards a harmonized segmentation protocol. *Neuroimage* **111**, 526–541 (2015).
14. van Strien, N. M., Cappaert, N. L. M. & Witter, M. P. The anatomy of memory: an interactive overview of the parahippocampal-hippocampal network. *Nat. Rev. Neurosci.* **10**, 272–282 (2009).
15. Hodgetts, C. J. *et al.* Ultra-High-Field fMRI Reveals a Role for the Subiculum in Scene Perceptual Discrimination. *The Journal of Neuroscience* vol. 37 3150–3159 (2017).
16. Berron, D. *et al.* Strong Evidence for Pattern Separation in Human Dentate Gyrus. *J. Neurosci.* **36**, 7569–7579 (2016).
17. Neunuebel, J. P. & Knierim, J. J. CA3 retrieves coherent representations from degraded input: direct evidence for CA3 pattern completion and dentate gyrus pattern separation. *Neuron* **81**, 416–427 (2014).
18. Plachti, A. *et al.* Multimodal Parcellations and Extensive Behavioral Profiling Tackling the

Hippocampus Gradient. *Cereb. Cortex* **29**, 4595–4612 (2019).
19. Strange, B. A., Witter, M. P., Lein, E. S. & Moser, E. I. Functional organization of the hippocampal longitudinal axis. *Nat. Rev. Neurosci.* **15**, 655–669 (2014).
20. Bienkowski, M. S. *et al.* Integration of gene expression and brain-wide connectivity reveals the multiscale organization of mouse hippocampal networks. *Nat. Neurosci.* **21**, 1628–1643 (2018).
21. Cenquizca, L. A. & Swanson, L. W. Spatial organization of direct hippocampal field CA1 axonal projections to the rest of the cerebral cortex. *Brain Res. Rev.* **56**, 1–26 (2007).
22. Kharabian Masouleh, S., Plachti, A., Hoffstaedter, F., Eickhoff, S. & Genon, S. Characterizing the gradients of structural covariance in the human hippocampus. *Neuroimage* **218**, 116972 (2020).
23. Nordin, K. *et al.* Structural whole-brain covariance of the anterior and posterior hippocampus: Associations with age and memory. *Hippocampus* **28**, 151–163 (2018).
24. Maass, A., Berron, D., Libby, L. A., Ranganath, C. & Düzel, E. Functional subregions of the human entorhinal cortex. *Elife* **4**, (2015).
25. Brunec, I. K. *et al.* Multiple Scales of Representation along the Hippocampal Anteroposterior Axis in Humans. *Curr. Biol.* **28**, 2129–2135.e6 (2018).
26. Chase, H. W. *et al.* Evidence for an anterior-posterior differentiation in the human hippocampal formation revealed by meta-analytic parcellation of fMRI coordinate maps: focus on the subiculum. *Neuroimage* **113**, 44–60 (2015).
27. Poppenk, J., Evensmoen, H. R., Moscovitch, M. & Nadel, L. Long-axis specialization of the human hippocampus. *Trends Cogn. Sci.* **17**, 230–240 (2013).
28. Henriksen, E. J. *et al.* Spatial representation along the proximodistal axis of CA1. *Neuron* **68**, 127–137 (2010).
29. Li, Q. *et al.* Human brain function during pattern separation follows hippocampal and neocortical connectivity gradients. doi:10.1101/2020.06.22.165290.
30. Przeździk, I., Faber, M., Fernández, G., Beckmann, C. F. & Haak, K. V. The functional organisation of the hippocampus along its long axis is gradual and predicts recollection. *Cortex* **119**, 324–335 (2019).
31. Vos de Wael, R. *et al.* Anatomical and microstructural determinants of hippocampal subfield functional connectome embedding. *Proc. Natl. Acad. Sci. U. S. A.* **115**, 10154–10159 (2018).
32. Haak, K. V. & Beckmann, C. F. Understanding brain organisation in the face of functional heterogeneity and functional multiplicity. *Neuroimage* **220**, 117061 (2020).
33. Huntenburg, J. M., Bazin, P.-L. & Margulies, D. S. Large-Scale Gradients in Human Cortical Organization. *Trends Cogn. Sci.* **22**, 21–31 (2018).
34. Margulies, D. S. *et al.* Situating the default-mode network along a principal gradient of macroscale cortical organization. *Proc. Natl. Acad. Sci. U. S. A.* **113**, 12574–12579 (2016).
35. Vogel, J. W. *et al.* A molecular gradient along the longitudinal axis of the human hippocampus informs large-scale behavioral systems. *Nature Communications* vol. 11 (2020).
36. Whelan, C. D. *et al.* Heritability and reliability of automatically segmented human hippocampal formation subregions. *Neuroimage* **128**, 125–137 (2016).
37. Patel, S. *et al.* Heritability of hippocampal subfield volumes using a twin and non-twin siblings design. *Hum. Brain Mapp.* **38**, 4337–4352 (2017).
38. van der Meer, D. *et al.* Brain scans from 21,297 individuals reveal the genetic architecture

of hippocampal subfield volumes. *Mol. Psychiatry* **25**, 3053–3065 (2020).
39. Van Essen, D. C. *et al.* The WU-Minn Human Connectome Project: an overview. *Neuroimage* **80**, 62–79 (2013).
40. Coifman, R. R. & Lafon, S. Diffusion maps. *Applied and Computational Harmonic Analysis* vol. 21 5–30 (2006).
41. Glasser, M. F. & Van Essen, D. C. Mapping human cortical areas in vivo based on myelin content as revealed by T1- and T2-weighted MRI. *J. Neurosci.* **31**, 11597–11616 (2011).
42. Paquola, C. *et al.* A multi-scale cortical wiring space links cellular architecture and functional dynamics in the human brain. *PLOS Biology* vol. 18 e3000979 (2020).
43. Almasy, L. & Blangero, J. Multipoint quantitative-trait linkage analysis in general pedigrees. *Am. J. Hum. Genet.* **62**, 1198–1211 (1998).
44. Caldairou, B. *et al.* A Surface Patch-Based Segmentation Method for Hippocampal Subfields. *Medical Image Computing and Computer-Assisted Intervention – MICCAI 2016* 379–387 (2016) doi:10.1007/978-3-319-46723-8_44.
45. Burt, J. B., Helmer, M., Shinn, M., Anticevic, A. & Murray, J. D. Generative modeling of brain maps with spatial autocorrelation. *Neuroimage* **220**, 117038 (2020).
46. Vos de Wael, R. *et al.* BrainSpace: a toolbox for the analysis of macroscale gradients in neuroimaging and connectomics datasets. *Commun Biol* **3**, 103 (2020).
47. Alexander-Bloch, A. F. *et al.* On testing for spatial correspondence between maps of human brain structure and function. *Neuroimage* **178**, 540–551 (2018).
48. Yeo, B. T. T. *et al.* The organization of the human cerebral cortex estimated by intrinsic functional connectivity. *Journal of Neurophysiology* vol. 106 1125–1165 (2011).
49. DeKraker, J., Köhler, S. & Khan, A. R. Surface-based hippocampal subfield segmentation. *Trends Neurosci.* **44**, 856–863 (2021).
50. Turnbull, A. *et al.* Author Correction: Reductions in task positive neural systems occur with the passage of time and are associated with changes in ongoing thought. *Sci. Rep.* **10**, 12941 (2020).
51. Bernhardt, B. C. *et al.* The spectrum of structural and functional imaging abnormalities in temporal lobe epilepsy. *Ann. Neurol.* **80**, 142–153 (2016).
52. Valk, S. L. *et al.* Genetic and phylogenetic uncoupling of structure and function in human transmodal cortex. doi:10.1101/2021.06.08.447522.
53. Arnatkeviciute, A. *et al.* Genetic influences on hub connectivity of the human connectome. *Nat. Commun.* **12**, 4237 (2021).
54. Haak, K. V. & Beckmann, C. F. Plasticity versus stability across the human cortical visual connectome. *Nat. Commun.* **10**, 3174 (2019).
55. Cooper, C. 'iana, Moon, H. Y. & van Praag, H. On the Run for Hippocampal Plasticity. *Cold Spring Harb. Perspect. Med.* **8**, (2018).
56. McEwen, B. S. STRESS AND HIPPOCAMPAL PLASTICITY. *Annual Review of Neuroscience* vol. 22 105–122 (1999).
57. Elman, J. A. *et al.* Genetic architecture of hippocampal subfields on standard resolution MRI: How the parts relate to the whole. *Hum. Brain Mapp.* **40**, 1528–1540 (2019).
58. Hibar, D. P. *et al.* Novel genetic loci associated with hippocampal volume. *Nat. Commun.* **8**, 13624 (2017).
59. Hibar, D. P. *et al.* Common genetic variants influence human subcortical brain structures. *Nature* **520**, 224–229 (2015).
60. Stein, J. L. *et al.* Identification of common variants associated with human hippocampal and

intracranial volumes. *Nat. Genet.* **44**, 552–561 (2012).
61. Maller, J. J. *et al.* Hippocampal volumetrics in treatment-resistant depression and schizophrenia: the devil's in de-tail. *Hippocampus* **22**, 9–16 (2012).
62. Adler, D. H. *et al.* Characterizing the human hippocampus in aging and Alzheimer's disease using a computational atlas derived from ex vivo MRI and histology. *Proc. Natl. Acad. Sci. U. S. A.* **115**, 4252–4257 (2018).
63. Alexander-Bloch, A., Raznahan, A., Bullmore, E. & Giedd, J. The convergence of maturational change and structural covariance in human cortical networks. *J. Neurosci.* **33**, 2889–2899 (2013).
64. Valk, S. L. *et al.* Shaping brain structure: Genetic and phylogenetic axes of macroscale organization of cortical thickness. *Sci Adv* **6**, (2020).
65. Paquola, C. *et al.* Microstructural and functional gradients are increasingly dissociated in transmodal cortices. *PLoS Biol.* **17**, e3000284 (2019).
66. Burt, J. B. *et al.* Hierarchy of transcriptomic specialization across human cortex captured by structural neuroimaging topography. *Nature Neuroscience* vol. 21 1251–1259 (2018).
67. Cahalane, D. J., Charvet, C. J. & Finlay, B. L. Modeling local and cross-species neuron number variations in the cerebral cortex as arising from a common mechanism. *Proc. Natl. Acad. Sci. U. S. A.* **111**, 17642–17647 (2014).
68. Fornito, A., Arnatkevičiūtė, A. & Fulcher, B. D. Bridging the Gap between Connectome and Transcriptome. *Trends Cogn. Sci.* **23**, 34–50 (2019).
69. Alexander-Bloch, A. F. *et al.* Human Cortical Thickness Organized into Genetically-determined Communities across Spatial Resolutions. *Cereb. Cortex* **29**, 106–118 (2019).
70. Chen, C.-H. *et al.* Genetic topography of brain morphology. *Proc. Natl. Acad. Sci. U. S. A.* **110**, 17089–17094 (2013).
71. Taupin, P. *The Hippocampus: Neurotransmission and Plasticity in the Nervous System*. (Nova Publishers, 2007).
72. Jabès, A., Lavenex, P. B., Amaral, D. G. & Lavenex, P. Postnatal development of the hippocampal formation: a stereological study in macaque monkeys. *J. Comp. Neurol.* **519**, 1051–1070 (2011).
73. Insausti, R., Cebada-Sánchez, S. & Marcos, P. Postnatal Development of the Human Hippocampal Formation. *Advances in Anatomy, Embryology and Cell Biology* (2010) doi:10.1007/978-3-642-03661-3.
74. Smallwood, J. *et al.* The neural correlates of ongoing conscious thought. *iScience* **24**, 102132 (2021).
75. Buzsáki, G. & Tingley, D. Space and Time: The Hippocampus as a Sequence Generator. *Trends Cogn. Sci.* **22**, 853–869 (2018).
76. Wagner, A. D., Shannon, B. J., Kahn, I. & Buckner, R. L. Parietal lobe contributions to episodic memory retrieval. *Trends Cogn. Sci.* **9**, 445–453 (2005).
77. Fanselow, M. S. & Dong, H.-W. Are the dorsal and ventral hippocampus functionally distinct structures? *Neuron* **65**, 7–19 (2010).
78. Save, E., Poucet, B., Foreman, N. & Buhot, M.-C. Object exploration and reactions to spatial and nonspatial changes in hooded rats following damage to parietal cortex or hippocampal formation. *Behavioral Neuroscience* vol. 106 447–456 (1992).
79. Corbetta, M. & Shulman, G. L. Spatial neglect and attention networks. *Annu. Rev. Neurosci.* **34**, 569–599 (2011).

80. Glasser, M. F. *et al.* The minimal preprocessing pipelines for the Human Connectome Project. *NeuroImage* vol. 80 105–124 (2013).
81. Patenaude, B., Smith, S. M., Kennedy, D. N. & Jenkinson, M. A Bayesian model of shape and appearance for subcortical brain segmentation. *NeuroImage* vol. 56 907–922 (2011).
82. Dale, A. M., Fischl, B. & Sereno, M. I. Cortical surface-based analysis. I. Segmentation and surface reconstruction. *Neuroimage* **9**, 179–194 (1999).
83. Fischl, B., Sereno, M. I. & Dale, A. M. Cortical Surface-Based Analysis. *NeuroImage* vol. 9 195–207 (1999).
84. Fischl, B., Sereno, M. I., Tootell, R. B. H. & Dale, A. M. High-resolution intersubject averaging and a coordinate system for the cortical surface. *Human Brain Mapping* vol. 8 272–284 (1999).
85. Van Essen, D. C., Glasser, M. F., Dierker, D. L., Harwell, J. & Coalson, T. Parcellations and hemispheric asymmetries of human cerebral cortex analyzed on surface-based atlases. *Cereb. Cortex* **22**, 2241–2262 (2012).
86. Glasser, M. F. *et al.* A multi-modal parcellation of human cerebral cortex. *Nature* **536**, 171–178 (2016).
87. Greve, D. N. & Fischl, B. Accurate and robust brain image alignment using boundary-based registration. *Neuroimage* **48**, 63–72 (2009).
88. Salimi-Khorshidi, G. *et al.* Automatic denoising of functional MRI data: combining independent component analysis and hierarchical fusion of classifiers. *Neuroimage* **90**, 449–468 (2014).
89. Kulaga-Yoskovitz, J. *et al.* Multi-contrast submillimetric 3 Tesla hippocampal subfield segmentation protocol and dataset. *Sci Data* **2**, 150059 (2015).
90. Styner, M. *et al.* Framework for the Statistical Shape Analysis of Brain Structures using SPHARM-PDM. *Insight J.* 242–250 (2006).
91. Kim, H. *et al.* Multivariate hippocampal subfield analysis of local MRI intensity and volume: application to temporal lobe epilepsy. *Med. Image Comput. Comput. Assist. Interv.* **17**, 170–178 (2014).
92. Marcus, D. S. *et al.* Informatics and data mining tools and strategies for the human connectome project. *Front. Neuroinform.* **5**, 4 (2011).
93. Kochunov, P. *et al.* Homogenizing Estimates of Heritability Among SOLAR-Eclipse, OpenMx, APACE, and FPHI Software Packages in Neuroimaging Data. *Front. Neuroinform.* **13**, 16 (2019).
94. Glahn, D. C. *et al.* Genetic control over the resting brain. *Proc. Natl. Acad. Sci. U. S. A.* **107**, 1223–1228 (2010).
95. Almasy, L., Dyer, T. D. & Blangero, J. Bivariate quantitative trait linkage analysis: pleiotropy versus co-incident linkages. *Genet. Epidemiol.* **14**, 953–958 (1997).

Supplementary Materials

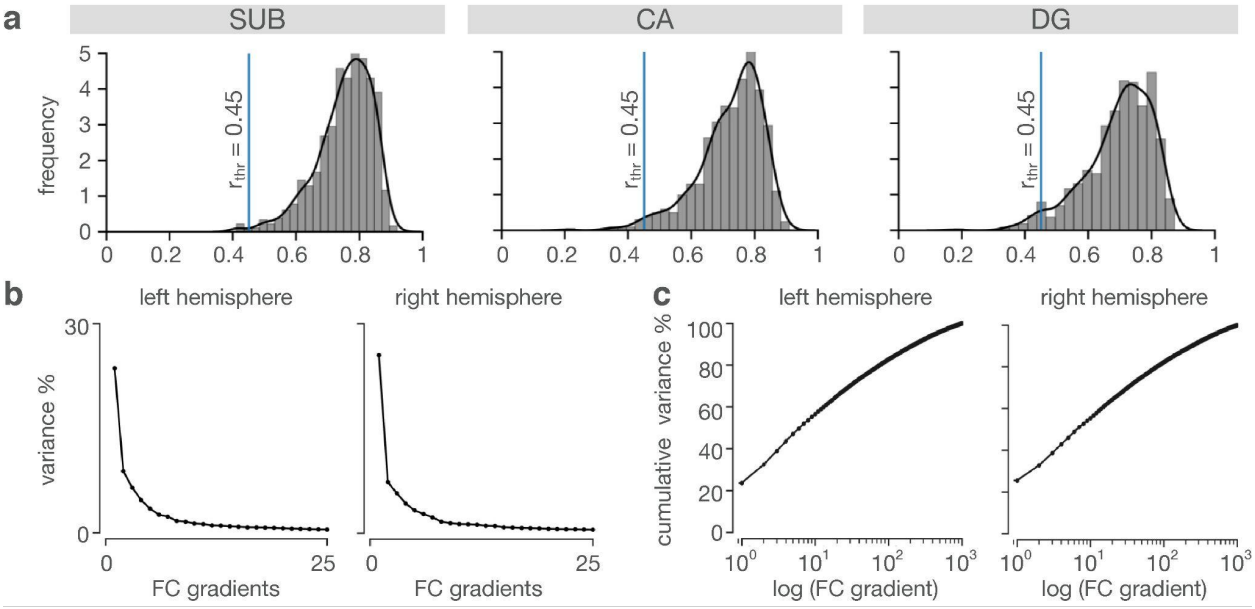

Supplementary Fig. S1. Similarity of individual hippocampal-isocortical FC maps to the group-level FC and variance explained by hippocampal FC gradients. a. FC similarity of n = 740 participants to the group-level FC quantified by means of Pearson's correlations (r). Threshold r-value (r_{thr} = 0.45) was assessed by computing the 2.5 standard deviation distance away from the mean r-values. Participants with a lower degree of similarity (r_{thr} < 0.45, n = 31) were excluded prior to the functional connectome gradients analysis. **b.** The first gradients explained 23.6% of total hippocampal-isocortical FC variance for the left hemisphere (left) and 25.5% for the right hemisphere (right). **c.** Cumulative variance explained by the first three gradients was 38.5% for the left hemisphere (left) and 38.9% for the right hemisphere (right).

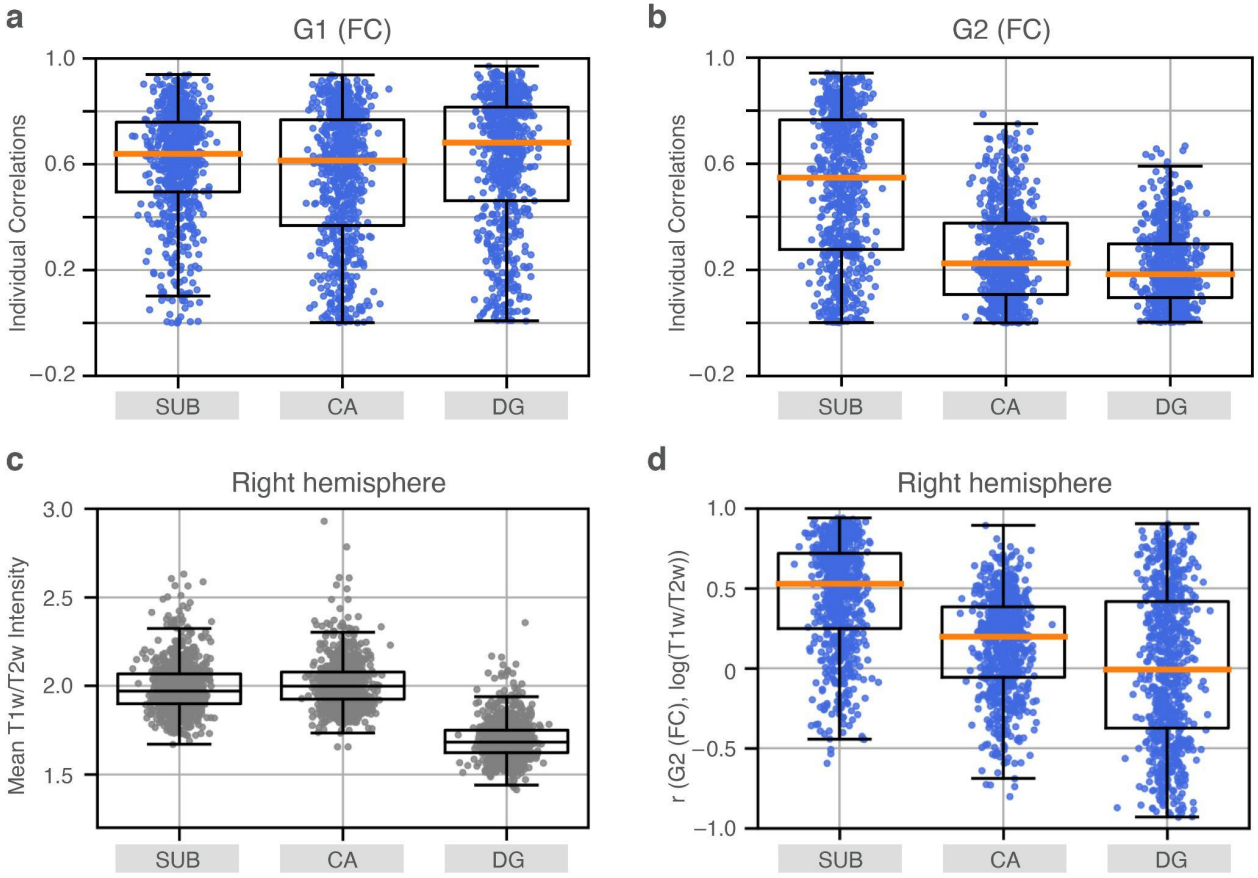

Supplementary Fig. S2. Quality assessment on primary and secondary functional gradients (G1 (FC), G2 (FC)) as well as T1w/T2w intensity maps. a. Pearson correlations between individual subjects' (n = 709) G1 (FC) maps and group-level G1 (FC) map for each subfield (SUB, CA, DG) in the left hemisphere. Individual correlations were significantly positive for the SUB (median $\bar{r}$ = 0.64, p < 0.001, one-tailed Wilcoxon signed-rank test), CA ($\bar{r}$ = 0.61, p < 0.001), and DG ($\bar{r}$ = 0.68, p < 0.001). **b.** Pearson correlations between individual subjects' G2 (FC) maps and group-level G2 (FC) map for each subfield in the left hemisphere. Individual correlations were significantly positive for the SUB ($\bar{r}$ = 0.55, p < 0.001), CA ($\bar{r}$ = 0.22, p < 0.001), and DG ($\bar{r}$ = 0.18, p < 0.001). **c.** Mean T1w/T2w intensity map distributions for each subject and each subfield in the right hemisphere. Mean and standard deviations of T1w/T2w maps were 1.99 ±0.43 for SUB, 2.01 ±0.68 for CA, and 1.69 ±0.23 for DG. **d.** Pearson correlations between individual subjects' G2 (FC) maps and T1w/T2w intensity maps for each subfield in the right hemisphere. Individual correlations were significantly positive for the SUB ($\bar{r}$ = 0.53, p < 0.001) and CA ($\bar{r}$ = 0.20, p < 0.001), however, not for DG ($\bar{r}$ = -0.01, p = 0.6).

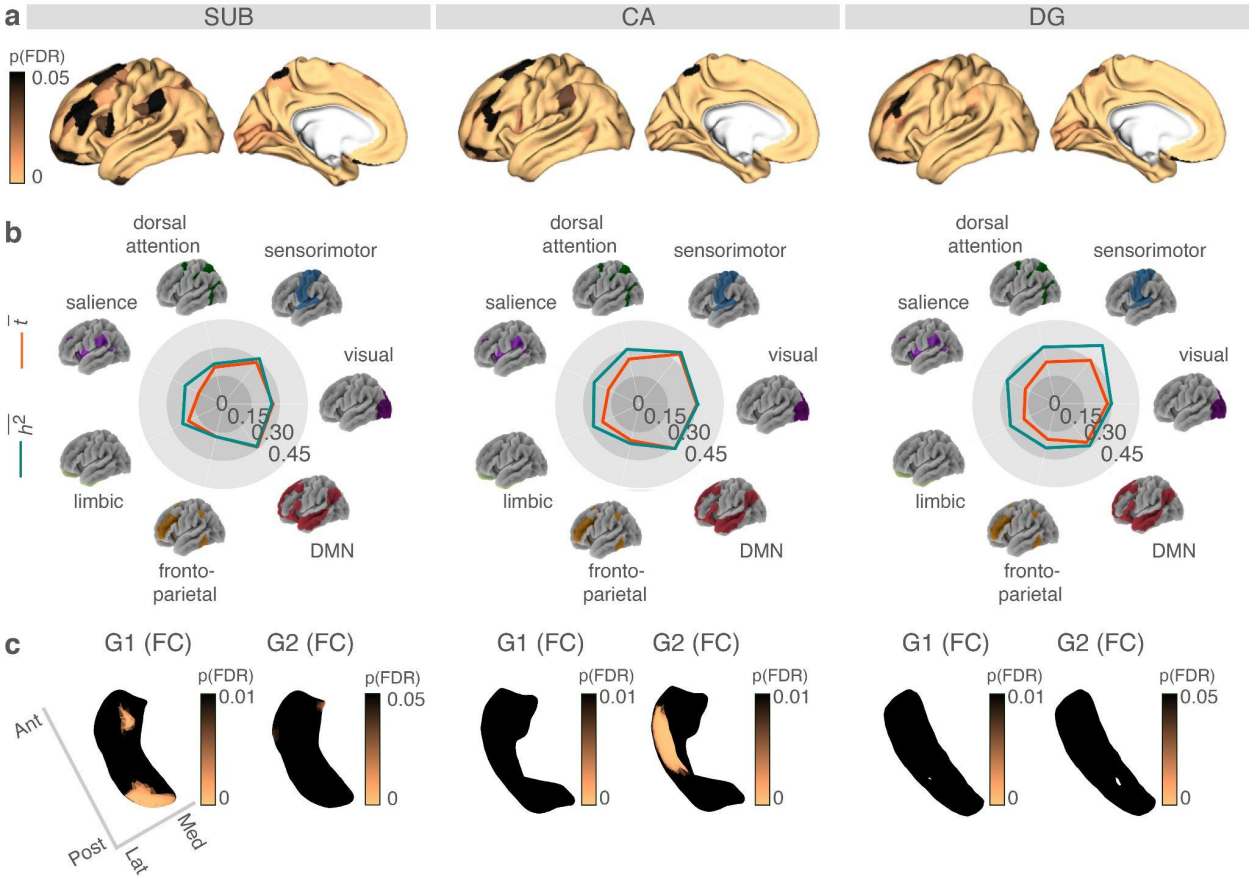

Supplementary Fig. S3. Significance levels of the isocortical heritability scores, network distribution of hippocampal-isocortical FC and its heritability, and the heritability of subfield FC gradients and T1w/T2w intensity maps. a. Heritability (h^2) scores of the hippocampal-isocortical FC in **Fig. 1c** were significant along most of the cortical regions for SUB, CA, and DG, as reported with the multiple comparison corrected p-values (p(FDR)). **b.** Isocortical-hippocampal FC strength and its heritability (t-values & h^2scores) distributed into seven networks [1] and averaged ($\bar{t}$ and $\overline{h^2}$). **c.** h^2-scores of the gradient maps were significant only for the SUB-G1 (FC) (anterior and posterior portions) and for the CA-G2 (FC) (lateral portions) as reported by the p(FDR) (copper color denotes pFDR < 0.05, black pFDR > 0.05).

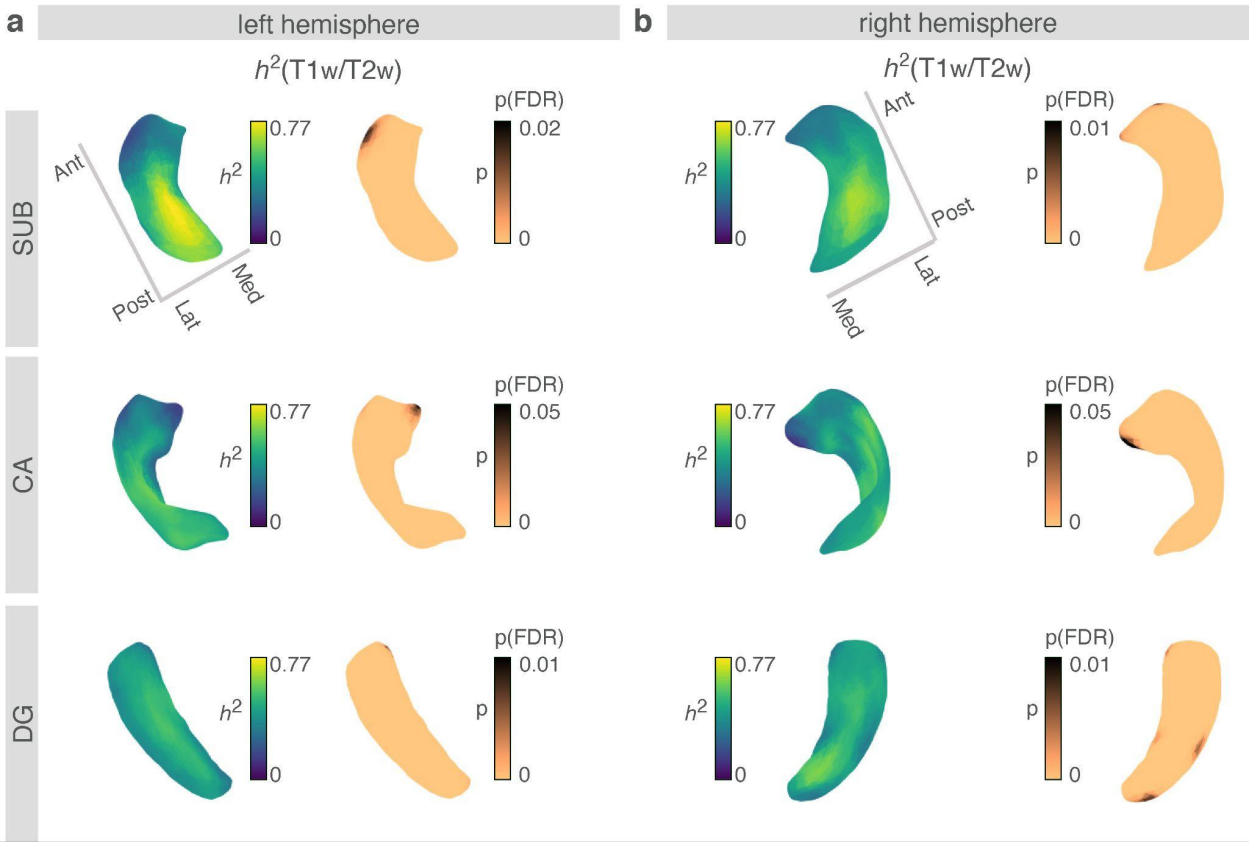

Supplementary Fig. S4. Heritability of the T1w/T2w intensity maps (h^2(T1w/T2w)) by controlling for the mean T1w/T2w intensities for each subfield (SUB, CA, DG) and hemisphere (left and right). **a.** h^2(T1w/T2w) patterns and their FDR-corrected significance levels (p(FDR)) did not change after controlling for the mean T1w/T2w intensities for the left hemisphere (copper color denotes pFDR < 0.05, black pFDR > 0.05). **b.** Similar results were observed for the right hemisphere.

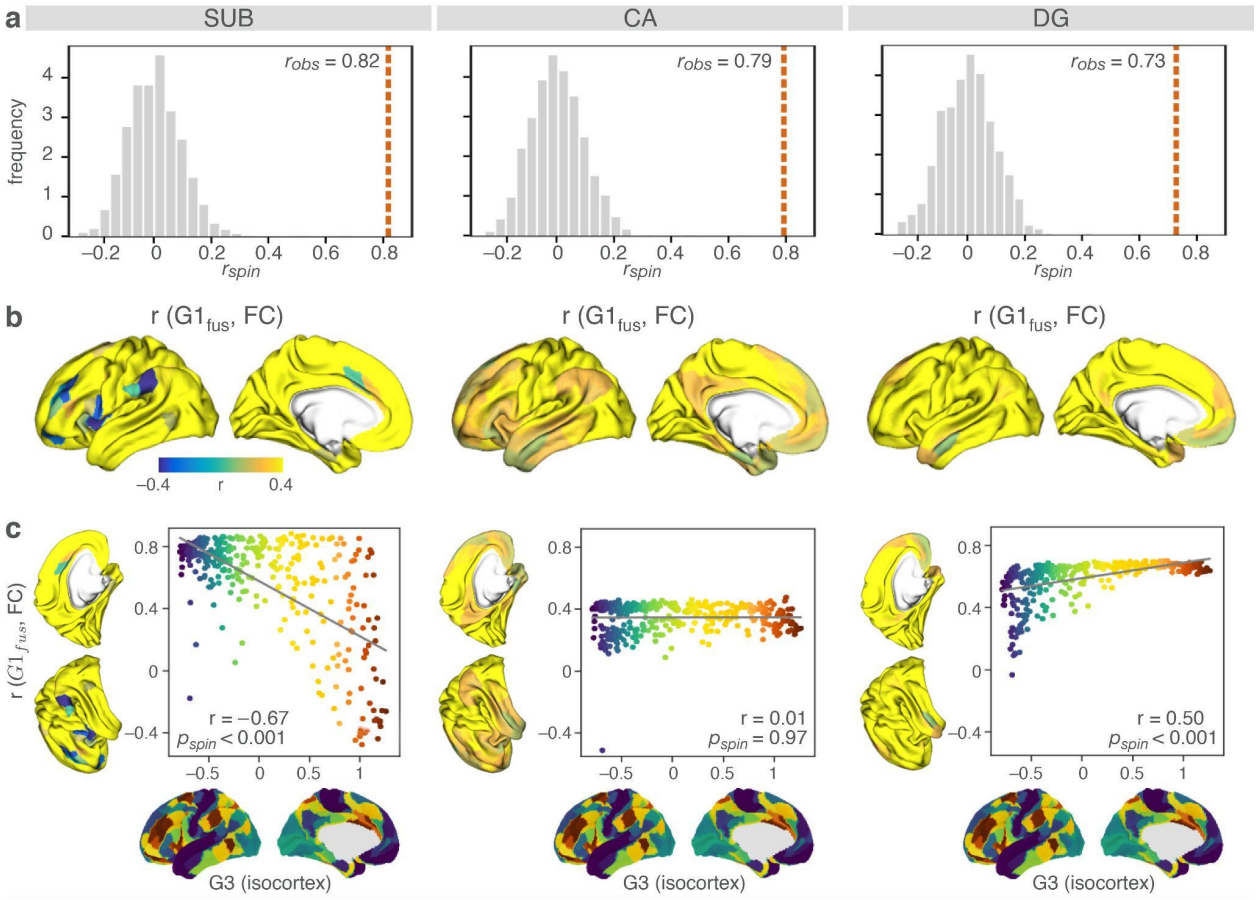

Supplementary Fig. S5. The association between the fused gradient projections and the third macroscale gradient. a. Significance level of correlations between r($G2_{fus}$,FC) and G3 (isocortex) from **Fig. 4e** assessed by the spin permutations [2,3], that controls for the spatial auto-correlations. Observed correlations r_{obs} correspond to the Pearson correlations between r($G2_{fus}$,FC) and G3 (isocortex) and spin correlations r_{spin} correspond to that of the shuffled data by accounting for the surface coordinates (n_{perm} = 1000). Significance levels are reported to be p_{spin}< 0.001 for all subfields SUB, CA, and DG. **b.** Variations in hippocampal-cortical FC across the principal fusion gradient ($G1_{fus}$) projected onto the isocortex (r-values). **c.** Regional associations between the whole-brain multiple demand gradient (G3 (isocortex)) and the r-values from Panel B (SUB: r = -0.67 and p_{spin}< 0.001, CA: r = 0.01 and p_{spin}= 0.97, DG: r = 0.50 and p_{spin}< 0.001).

LSUB	G1 (FC)	G1 (SiC)	G2 (FC)	G2 (SiC)
$G1_{fus}$	r = -0.29, p_{vario} = 0.02	r = -0.09, p_{vario} = 0.42	r =0.46, p_{vario} = 0.001	r =0.39, p_{vario} = 0.01
$G2_{fus}$	r = 0.89, p_{vario} < 0.001	r = 0.78, p_{vario} < 0.001	r = 0.12, p_{vario} = 0.37	r = 0.03, p_{vario} = 0.83

LCA	G1 (FC)	G1 (SiC)	G2 (FC)	G2 (SiC)
$G1_{fus}$	r = 0.29, p_{vario} = 0.002	r = 0.17, p_{vario} = 0.07	r = 0.14, p_{vario} = 0.11	r =0.74, p_{vario} < 0.001
$G2_{fus}$	r = 0.89, p_{vario} < 0.001	r = 0.89, p_{vario} < 0.001	r = 0.21, p_{vario} = 0.04	r = -0.18, p_{vario} = 0.07

LDG	G1 (FC)	G1 (SiC)	G2 (FC)	G2 (SiC)
$G1_{fus}$	r = 0.53, p_{vario} < 0.001	r = 0.41 and p_{vario} = 0.003	r = 0.22, p_{vario} = 0.03	r = 0.36, p_{vario} = 0.004
$G2_{fus}$	r = 0.86, p_{vario} < 0.001	r = 0.83, p_{vario} < 0.001	r = -0.26, p_{vario} = 0.04	r = 0.25, p_{vario} = 0.06

Supplementary Table S1. The association between the fused gradient projections and FC and SiC hippocampal gradients.

LSUB	G1 (isocortex)	G2 (isocortex)	G3 (isocortex)
r ($G1_{fus}$, FC)	r = 0.02, p_{spin} = 0.81	r = -0.17, p_{spin} = 0.31	r = -0.67, p_{spin} < 0.001
r ($G2_{fus}$, FC)	r = -0.06, p_{spin} = 0.60	r = -0.01, p_{spin} = 0.97	r = 0.82, p_{spin} < 0.001

LCA	G1 (isocortex)	G2 (isocortex)	G3 (isocortex)
r ($G1_{fus}$, FC)	r = -0.70, p_{spin} < 0.001	r = 0.04, p_{spin} = 0.85	r = 0.01, p_{spin} = 0.97
r ($G2_{fus}$, FC)	r = -0.30, p_{spin} = 0.002	r = -0.05, p_{spin} = 0.73	r = 0.79, p_{spin} < 0.001

LDG	G1 (isocortex)	G2 (isocortex)	G3 (isocortex)
r ($G1_{fus}$, FC)	r = -0.54, p_{spin} < 0.001	r = -0.08, p_{spin} = 0.57	r = 0.50, p_{spin} < 0.001
r ($G2_{fus}$, FC)	r = -0.48, p_{spin} < 0.001	r = -0.03, p_{spin} = 0.81	r = 0.73, p_{spin} < 0.001

Supplementary Table S2. The association between the fused gradient projections and the macroscale isocortical gradients.

References

1. Yeo, B. T. T. *et al.* The organization of the human cerebral cortex estimated by intrinsic functional connectivity. *Journal of Neurophysiology* vol. 106 1125–1165 (2011).
2. Vos de Wael, R. *et al.* BrainSpace: a toolbox for the analysis of macroscale gradients in neuroimaging and connectomics datasets. *Commun Biol* **3**, 103 (2020).
3. Alexander-Bloch, A. F. *et al.* On testing for spatial correspondence between maps of human brain structure and function. *Neuroimage* **178**, 540–551 (2018).